Engineering Structures 195 (2019) 382–399

Contents lists available at ScienceDirect

Engineering Structures

journal homepage: www.elsevier.com/locate/engstruct

Seismic performance upgrade of RC frame buildings using precast bolt-connected steel-plate reinforced concrete frame-braces

Xu-Yang Cao[a], De-Cheng Feng[a,b,c], Gang Wu[a,b,c,*]

[a] School of Civil Engineering, Southeast University, Nanjing 210096, China
[b] Key Laboratory of Concrete and Prestressed Concrete Structures of the Ministry of Education, Southeast University, Nanjing 210096, China
[c] Laboratory of Industrialized Structural and Bridge Engineering of Jiangsu Province, Southeast University, Nanjing 210096, China

ARTICLE INFO

Keywords:
Outside strengthening
Sub-structure
Precast
Steel-plate
Numerical model
Design procedure
Seismic upgrade
Dynamic response

ABSTRACT

This paper presents a new strengthening method for existing frames by using outside sub-structures, namely, precast bolt-connected steel-plate reinforced concrete (PBSPC) frame-braces. The working principles, numerical methods, and design procedures are presented, and case studies are carried out. The simulation results were consistent with the results from previous experiments, indicating the effectiveness of the numerical model. The design objective and procedure were put forward, and during the process, a coefficient η that considers the precast influences was considered. A practical engineering retrofitting was performed based on the proposed numerical model and design process, where the structure was subjected to the design basis earthquake (DBE) and maximum considered earthquake (MCE). The analyses demonstrated that the structural demands were clearly reduced within the thresholds, and the inner force was transferred from the existing building to the external sub-structure after strengthening. The incremental dynamic analysis (IDA) and fragility curves were plotted, illustrating the greater reliability in structural capacity and the lesser possibility of structural damage with the new upgrading form.

1. Introduction

Surveys of historical earthquakes have shown that old buildings without seismic upgrades are prone to severe damage during the hazards, and the collapse probability is extremely high, especially in high-intensity areas. In contrast, slight damage and lower collapse probability have been observed for structures after retrofitting, greatly reducing the property loss and casualties caused by strong earthquakes. In view of the large amounts of old structures in rural areas and the frequent occurrences of earthquake disasters in recent years, the importance of seismic performance upgrading as well as seismic capacity improvement has been put forward to a new height [1–3].

The existing upgrading techniques tend to focus more on component-level performance enhancements (e.g., wrapping with fibre-reinforced polymer (FRP) [4], enlarging section areas [5], bonding steel plate externally [6], replacing concrete and reinforcement [7]), which have played a role in improving the structural stiffness and strength and have been validated by practical projects. However, these retrofitting methods generally cause individual components to be stronger, and the integrity improvement of the whole structure (e.g. the overall force/displacement pattern change) is not obvious, especially for the structures considering the soft storey effect [8,9].

As the applications of seismic repair become wider and wider, various new reinforcing technologies are emerging, among which external sub-structure upgrading methods have been studied in Japan since the 1970s and enable a strengthening process on the structural-system-level [10–12]. The external sub-structure upgrading methods aim at improving the overall seismic performance of the whole structure, ameliorating the existing force/displacement pattern and transferring structural damage from the existing structure to the external sub-structure. All the construction work of the external sub-structure is carried out outside the existing building, mostly without entering the interior, which has significant economic benefits for institutions such as schools and hospitals whose operations cannot be interrupted. A variety of specific external forms are derived from the upgrading method, the most typical ones of which are the external framed steel brace [13], external parallel cable-stayed steel rod [14] and external reinforced concrete frame (RCF) [15], as shown in Fig. 1.

Because of the diagonal members in both the framed steel brace and parallel cable-stayed steel rod, the lateral stiffness of the outside sub-structure is increasingly enhanced. However, the steel structure is prone to rusting and buckling and has a lower high-temperature resistance,

* Corresponding author at: School of Civil Engineering, Southeast University, Nanjing 210096, China.
E-mail addresses: caoxy@seu.edu.cn (X.-Y. Cao), dcfeng@seu.edu.cn (D.-C. Feng), g.wu@seu.edu.cn (G. Wu).

https://doi.org/10.1016/j.engstruct.2019.06.007
Received 10 January 2019; Received in revised form 1 April 2019; Accepted 4 June 2019
0141-0296/ © 2019 Elsevier Ltd. All rights reserved.

(a) external framed steel brace (b) external parallel cable-stayed rod (c) external reinforced concrete frame

Fig. 1. Typical external sub-structure forms.

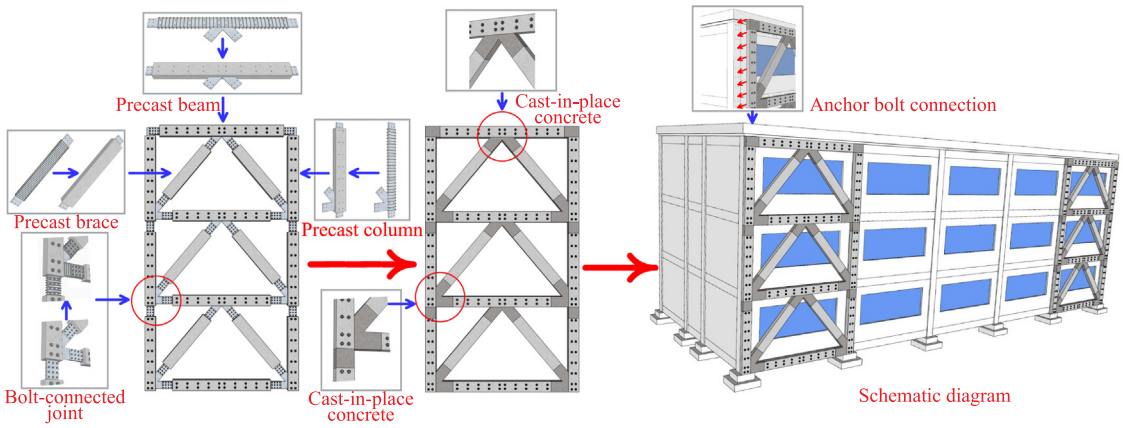

Fig. 2. Working Principle of PBSPC frame-brace.

which requires additional regular maintenance. The idea of energy dissipation has also been considered, and various types of new braces (e.g., the buckling restrained brace, the self-centering brace) have been investigated to substitute for the conventional steel brace, further improving the seismic capacity of the outside sub-structure [16,17]. However, due to its relatively high initial cost [18], it may not be suitable for the large number of rural buildings in China.

Comparatively, the external RCF possesses certain advantages of a lower price, better fire resistance and wider lighting performance, but its seismic bearing capacity is generally lower than that of the other forms for it has no braces. Although there have been attempts to attach RC braces to the external RCF [19], the practical construction process of the external sub-structure is almost cast-in-place with long periods. Because of the dense reinforcement ratio, the component quality is difficult to guarantee, which reduces the upgrading effect to some extent. The precast-assembly technology possess the superiority of mass production, rapid construction and quality assurance, having been promoted for decades mainly in new construction. However, the relevant research and applications in seismic repair and upgrading are relatively scarce [20,21].

In this paper, a new type of outside sub-structure, namely, the precast bolt-connected steel-plate reinforced concrete (PBSPC) frame-brace, is put forward, which combines the external sub-structure and precast-assembly technology. The working principles, simulation methods, and design procedures are presented, and case studies are carried out. The simulation results matched well with experiments conducted previously, which indicated that the numeric model may be suitable for the new upgrading form. The design objective and procedure were raised, and a coefficient η that considers the precast influences was calibrated by both simulation and experimental results. The case study, based on the proposed numerical model and design process, was analysed under the DBE and MCE, and the IDA and fragility curves were plotted afterwards. The seismic responses were clearly reduced below the thresholds after strengthening, and the original structure became more reliable for all performance levels with the new upgrading form.

2. Working principle

The precast bolt-connected steel-plate reinforced concrete (PBSPC) frame-brace sub-structure shown in this paper is formed with precast components including beams, columns and braces, all reinforced with steel plates. All the components are prefabricated ahead of time and transported to the site for assembly. Each precast member is connected mutually by high-strength friction bolts and steel plates stretching out of the component ends. The connecting joints are finally covered with cast-in-place concrete to protect the inner steel plate and form the integrated PBSPC frame-brace. The outside sub-structure connects with the existing structure by anchor-bolts, which penetrates through the pre-opening holes of precast components and anchors into the inner structure. The gap between them is further filled by bonding mortar to guarantee the combination. Fig. 2 shows the general upgrade principle and assembly process of a typical inverted V-shaped PBSPC frame-brace.

In comparison with the direct attachment of the brace to the existing RCF, the PBSPC frame-brace has its own advantages. On the one hand, it strengthens the existing beam and column simultaneously because the outside beam and column can be regarded as an equivalent enlargement of the inner sections. On the other hand, the outside sub-structure provides a place for the additional brace, which effectively prevents damage to the joints of the existing RCF, as large force shall be transferred from the additional brace to the joint zones.

The PBSPC frame-brace sub-structure works together with the existing RCF during an earthquake and improves the overall performance, altering the force-transfer mechanisms and providing upgrades on the structural-system level. The prefabrication process and assembly

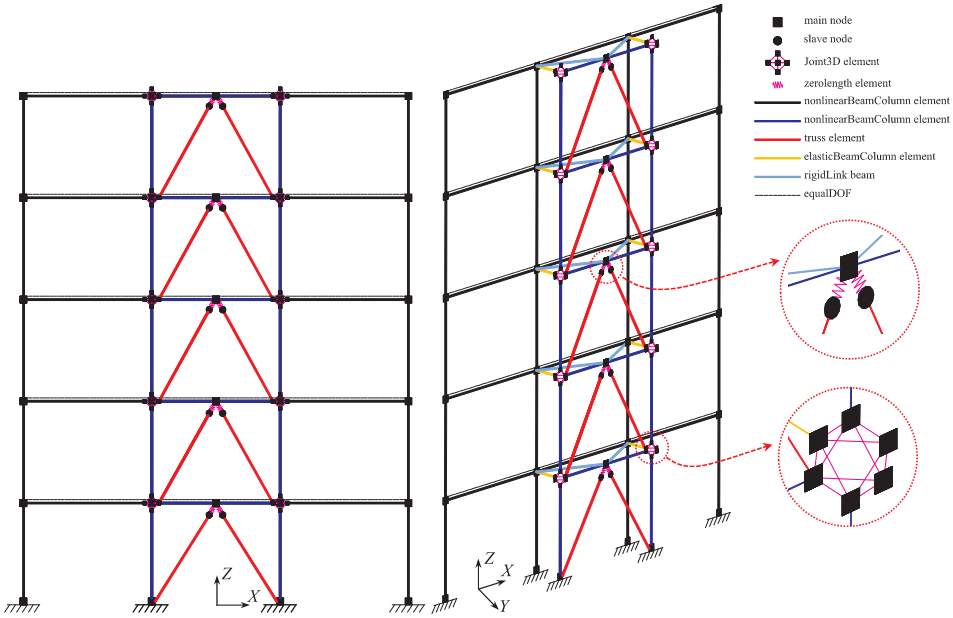

Fig. 3. 3D numerical model for PBSPC frame-brace.

technology ensure the components' quality while reducing the strengthening period. The precast brace greatly improves the lateral stiffness and bearing capacity of the whole structure, playing a major role in the upgrading form.

3. Numerical simulation method

To investigate the behaviours of the existing RCF strengthened with the PBSPC frame-brace sub-structure, a 3D numerical model is proposed using OpenSees software (Open System for Earthquake Engineering Simulation) (Fig. 3) [22,23]. Different types of element models and material models are adopted to reflect the structural characteristics and enhance the fitting accuracy. The relevant element and material models used are as follows.

3.1. NonlinearBeamColumn element & fibre section model

Both the beams and columns of the existing RCF and outside PBSPC frame-brace are modelled by the NonlinearBeamColumn element, which is one of the most commonly used elements in OpenSees based on the flexibility method. The internal force distribution tends to be relatively stable, and the static equilibrium condition of the element is strictly satisfied even under strongly nonlinear conditions, so the mechanical behaviour of the entire beam and column members can be described using fewer elements. The NonlinearBeamColumn element is set with a plurality of integration points along the length direction, and each integral point characterizes the section at the place [24,25].

The fibre cross model is considered to describe the force-deformation relationship of the section, as shown in Fig. 4(a). The concrete fibre and steel fibre are assigned to have the Concrete02 material model and Steel02 material model, respectively (Fig. 4(b) and (c)). The compression part of the Concrete02 material model is based on the Kent-Park model consisting of three parts. The hoop effect of the stirrups on the strength and ductility of the concrete can also be reflected by introducing a strengthening coefficient [26], with a recommended value of 1.2–1.3. The Steel02 material model possesses higher computational efficiency due to its explicit algorithm. In addition, the Bausinger effect can be reflected, which is quite important, especially in cyclic loading.

3.2. Joint3D element & Pinching4 material model

As the beam-column joint zones are the main parts of the PBSPC frame-brace and have a critical function in the whole structures, special consideration has been given to analysing their influence [27,28]. Different types of joint elements have been proposed in OpenSees (e.g., scissors model, BeamColumnJoint model and Joint2D model), and in this modelling of the PBSPC frame-brace, the Joint3D element [29] was adopted (Fig. 5), which is defined in a three-dimensional domain with six external nodes and one central node. The central node controls both the rigid body motion and shear deformation of the element with its nine degrees of freedom (i.e., six degrees for the rigid-body motion and three degrees for shear distortion).

Three uniaxial material models characterize the three shear deformation modes of the joint block in three directions, and in this paper, the Pinching4 material model was assigned. Modified compression field theory (MCFT) [30] is adopted to calculate the control point values of the Pinching4 material based on Membrane software (Fig. 6) [31]. The Pinching4 material model can also reflect the damage developments such as strength degradation, stiffness degradation and pinching effect. The parameter values of Pinching4 material model are listed in Table 1 for reference.

3.3. Zerolength element & Hysteretic material model

The brace-beam joint zones of the PBSPC frame-brace have an immense impact on the brace performance, further changing the structural lateral stiffness and causing out-of-plane instability, so the zerolength element is particularly used between the brace end node and beam middle node. The degrees of freedom of the two nodes are all bonded (i.e., equalDOF constraint), except for the bending degree of freedom along axis y. The unit-length fibre section analysis is conducted to obtain the moment-rotation relationship along axis y, and during the process, the effects of the steel plate bond-slip as well as post-cast concrete grade are analysed (Fig. 7) [32,33].

The key point values of the generated moment-rotation relationship are selected for the hysteretic material model, which is assigned to the zerolength element. The hysteretic material model can reflect the pinching effect during reloading, stiffness degradation during unloading and damage due to energy dissipation. The parameter values of Hysteretic material model are listed in Table 1 for reference.

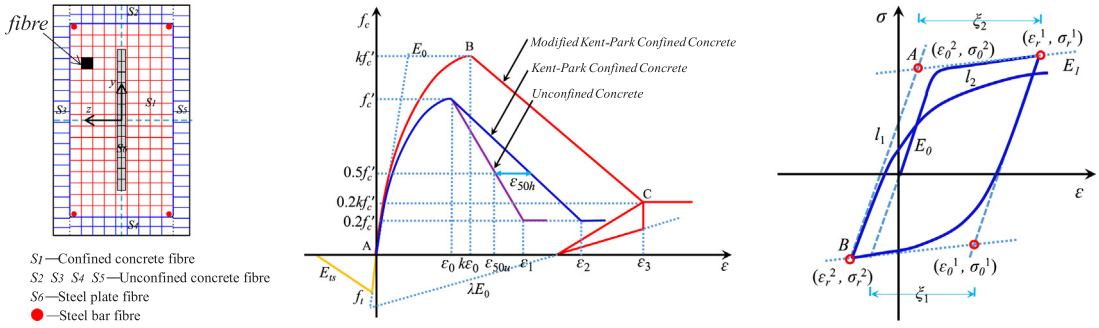

(a) fibre cross section (b) Concrete02 constitutive model (c) Steel02 constitutive model

Fig. 4. Beam and column simulation.

3.4. Truss element & rigid element & multipoint constraints

To model the precast brace of the outside PBSPC sub-structure, the truss element was adopted in view of the much larger axial force compared with other inner forces. The fibre section model was also used for the truss element as mentioned before. Due to the redundancy of the anchor bolts in the design process, the interfaces between the outside sub-structure and the existing RCF were regarded to be firmly connected, so the rigid element (i.e., elastic beam-column elements) and multipoint constraint (i.e., rigidLink constraint) were selected to reflect the connecting performance. The elastic beam-column elements were set between the outer sub-structure joints and the inner RCF joints, while rigidLinks were constrained between the outer beam middle points and the corresponding RCF joints. Under the assumption of the rigid floor, the two outer ends of the existing RCF beams were bound to limit the displacements in the axis x direction, using the equalDOF constraints [28,34].

3.5. Model verification

The proposed simulation method was preliminarily validated using three cyclic load tests previously conducted at Southeast University (i.e., RCF without strengthening, RCF strengthened with the V-shaped PBSPC frame-brace and RCF strengthened with the inverted V-shaped PBSPC frame-brace) [35]. As the experimental results of the V-shaped and inverted V-shaped PBSPC frame-braces were almost identical, only the inverted V-shaped sub-structure is considered for verification in this paper, as shown in Fig. 8. The mechanical properties of the concrete and steel for the experiments are listed in Table 2.

Fig. 9(a) and (b) show the load-displacement relationship before and after strengthening, while Fig. 9(c) and (d) present the load-strain relationship before and after strengthening. In general, the simulation model results match well with the experimental results and show high fitting accuracy in the peak load, stiffness degradation and strength degradation, which indicates that the proposed numerical model may be suitable to simulate the PBSPC frame-brace upgrading form [36,37].

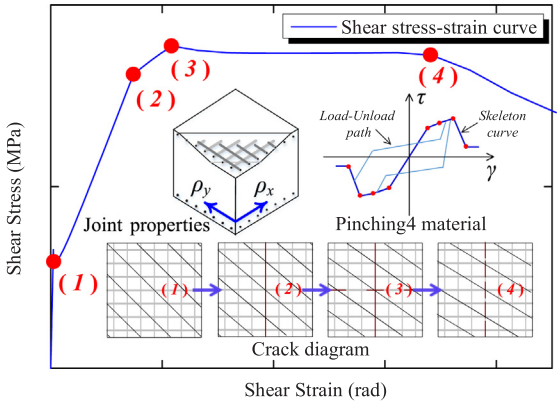

Fig. 6. Acquiring the control point values of Pinching4 material based on Membrane software.

4. Design procedure

4.1. Design objectives

In this study, a stiffness-based design procedure is used, and two levels of ground motions are considered (i.e., the DBE and MCE levels). The outside PBSPC frame-brace substructure is designed using the DBE level, and the structural responses are calculated under both the DBE and MCE. To evaluate the seismic performances and related damage conditions of the structural system after strengthening, two limit states are adopted, the immediate occupancy (IO) for the DBE level and the life safety (LS) level for the MCE level [38,39]. The design objectives of the strengthening method with the PBSPC frame-brace are defined as

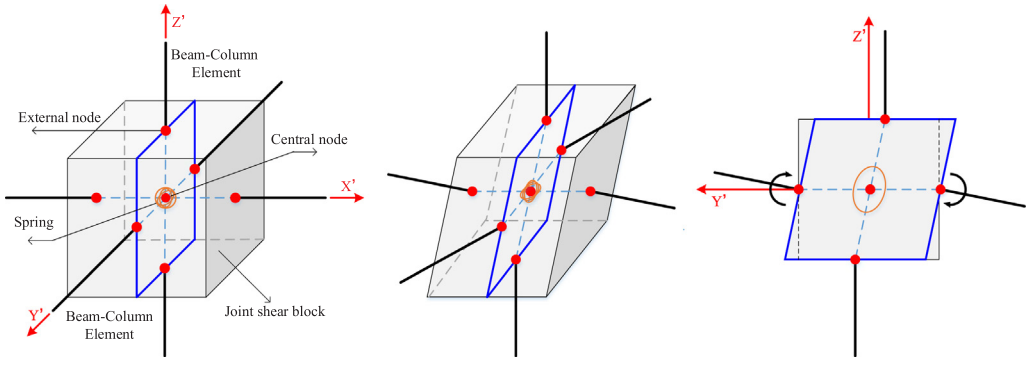

Fig. 5. Joint3D element model.

Table 1
Parameter values in Pinching4 material and Hysteretic material.

Pinching4 material		Hysteretic material	
Unload-reload path	[0.15,0.15;0.15,0.15;0.0,0.0]	Pinching (deformation) during reloading	1
Unloading stiffness degradation	[1.30,0.0,0.10,0.0,5.5]	Pinching (force) during reloading	1
Reloading stiffness degradation	[0.12,0.0,0.9,0.0,0.95]	Unloading stiffness degradation	0.5
Strength degradation	[1.11,0.0,0.32,0.1,0.125]	Damage (ductility)	0
Damage (energy)	10	Damage (energy)	0.2

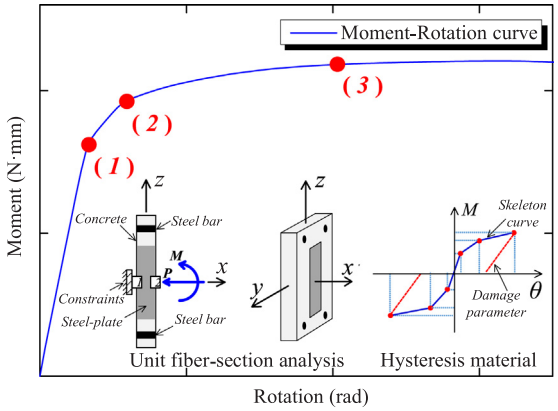

Fig. 7. Acquiring the control point values of hysteretic material model by the unit-length fibre section analysis.

follows:

Under the DBE level, the whole structure after strengthening shall satisfy the IO performance level. The overall damage level is light, and the possibility of personal and property safety being compromised is very low. Minor spalling occurs in a few places on the outside precast braces. The maximum transient inter-storey drift ratio shall not exceed 0.5% in the conservative consideration (the value is 1% for concrete frames and 0.5% for braced steel frames, as recommended in FEMA356 [38]).

Under the MCE level, the whole structure after strengthening shall satisfy the LS performance level. The overall damage level is moderate. Significant damage to the structure has occurred, centring on the outside PBSPC frame-braces. Many braces yield or buckle but do not totally fail. Damage has occurred to the nonstructural components of the existing RCF. The maximum transient inter-storey drift ratio shall not exceed 1.5% in the conservative consideration (the value is 2% for concrete frames and 1.5% for braced steel frames, as recommended in FEMA356 [38]).

4.2. Design process

According to the preceding design objectives, the stiffness-based design procedure of the outside strengthening method with the PBSPC frame-brace is summarized as follows (Fig. 10).

Step 1: According to the type of site, the intensity of the fortification, building conditions, etc., the sub-structure layout and the cross-sectional dimensions of the PBSPC frame-brace members are initially determined.
Step 2: The spatial three-dimensional structure after upgrading is converted into a planar two-dimensional structure [40]. The existing RCFs are merged into integrated one-span RCFs, while the outside PBSPC frame-braces are merged into integrated one-span PBSPC frame-braces. The total weight of the whole structures is calculated to obtain the first period of the structure.
Step 3: With the target spectrum of the DBE, the linear-elastic base shear demand, Q_d is obtained. Meanwhile, the response modification factor R is adopted to consider the structural ductility effect, and its value is selected to be 5, as recommended for concentrically braced frames in IBC [41]. The design base shear demand, V_d, is calculated thereafter by Eq. (1).

$$V_d = \frac{Q_d}{R} \tag{1}$$

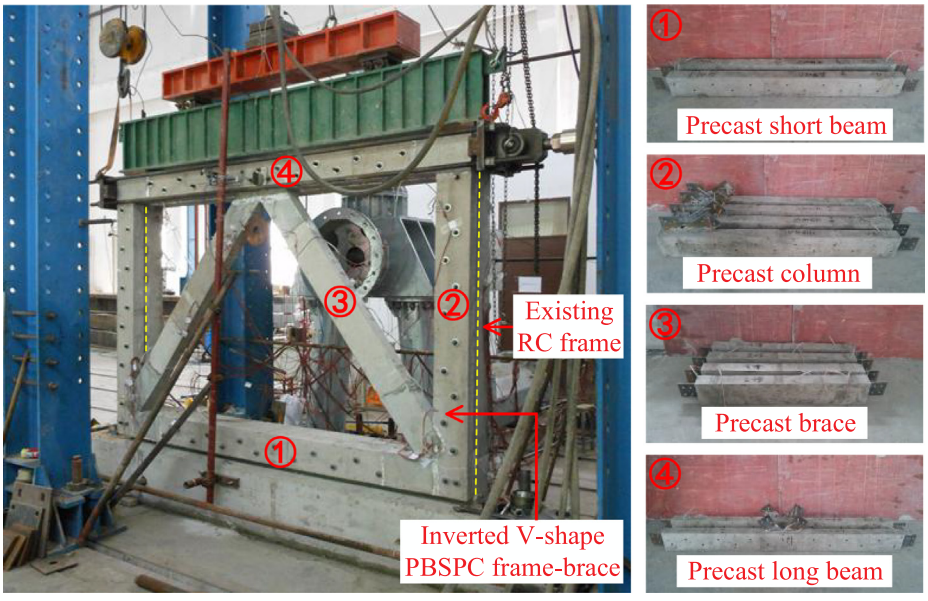

Fig. 8. PBSPC frame-brace sub-structure experiments conducted at Southeast University (inverted V-shaped).

Table 2
The mechanical properties of the concrete and steel for the experiments.

Item	Yield strength (MPa)	Ultimate strength (MPa)	Elastic modulus (GPa)
Stirrup	450	616	196
Longitudinal bar (existing RCF beam)	435	567	204
Longitudinal bar (existing RCF column)	366	504	200
Steel plate	275	410	189

Step 4: To distribute the design base shear demand to different stories, the equivalent base shear procedure (EBSP) recommended by GB50011 [39] is adopted, which is mainly applied to buildings less than 40 metres high with a uniform mass distribution. The principle of the EBSP is quite the same as the equivalent lateral force procedure (ELFP) recommended in ASCE/SEI 7-10 [42]. Thus,

$$P_n = \frac{G_n H_n}{\sum_{n=1}^{m} G_n H_n} \cdot (1-\delta) \cdot V_d \quad (n = 1, 2, \ldots, m) \tag{2}$$

where m equals the total stories; P_n, G_n and H_n represent the design shear demand, the weight and the height of the nth floor, respectively; and δrepresents the additional seismic coefficient of the top floor in consideration of the high-order mode effect [39].

Step 5: To obtain the design shear demand of each component, the lateral stiffness of each brace K_{brace} and column K_{column} is determined by Eqs. (3) and (4), respectively [39,43].

$$K_{brace} = (1-\lambda) \cdot \sin\theta \cdot \cos^2\theta \cdot \frac{E_b A_b}{h} \tag{3}$$

$$K_{column} = \frac{12 E_c I_c}{h^3} \cdot \alpha_c \tag{4}$$

where λ represents a coefficient considering the reduction effect of the axial deformation of the columns on the brace lateral stiffness, and the expression is shown in Eq. (5); α_c represents a coefficient considering the reduction effect of the bending deformation of the beams on the column lateral stiffness, which is related to the ratio of the line stiffness between the beam and column. α_c is denoted differently for the first floor and the others, as displayed in Eq. (6).

$$\lambda = \frac{\sin^2\theta}{\sin^2\theta + \frac{E_c A_c L}{E_b A_b h}} \tag{5}$$

$$\alpha_c = \begin{cases} \frac{0.5+\bar{i}}{2+\bar{i}}, \ \bar{i} = \frac{i_{b-l}^1 + i_{b-r}^1}{i_c^1}, & n = 1 \\ \frac{\bar{i}}{2+\bar{i}}, \ \bar{i} = \frac{i_{b-l}^n + i_{b-r}^n + i_{b-l}^{n-1} + i_{b-r}^{n-1}}{2 i_c^n}, & n = 2, 3 \ldots, m \end{cases} \tag{6}$$

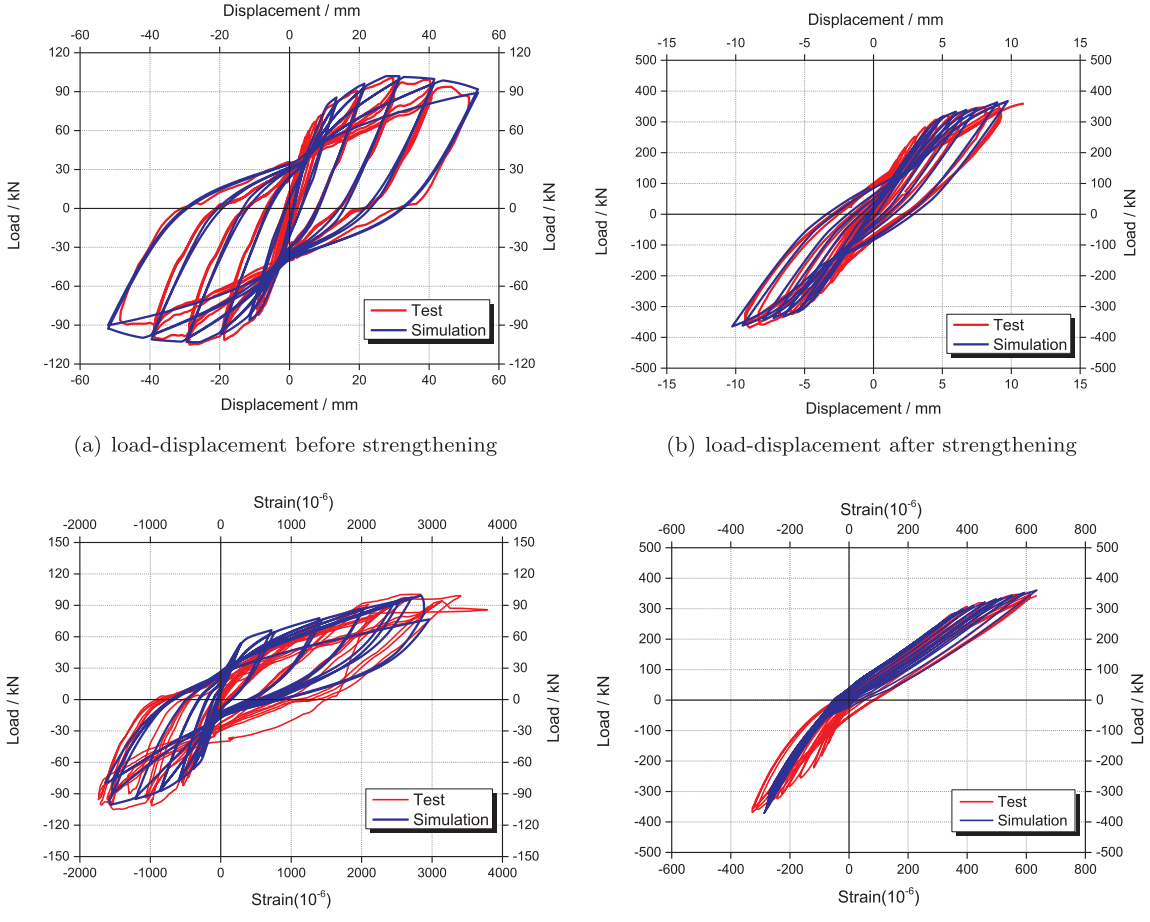

(a) load-displacement before strengthening

(b) load-displacement after strengthening

(c) load-strain before strengthening

(d) load-strain after strengthening

Fig. 9. Model verification between test and numerical curves.

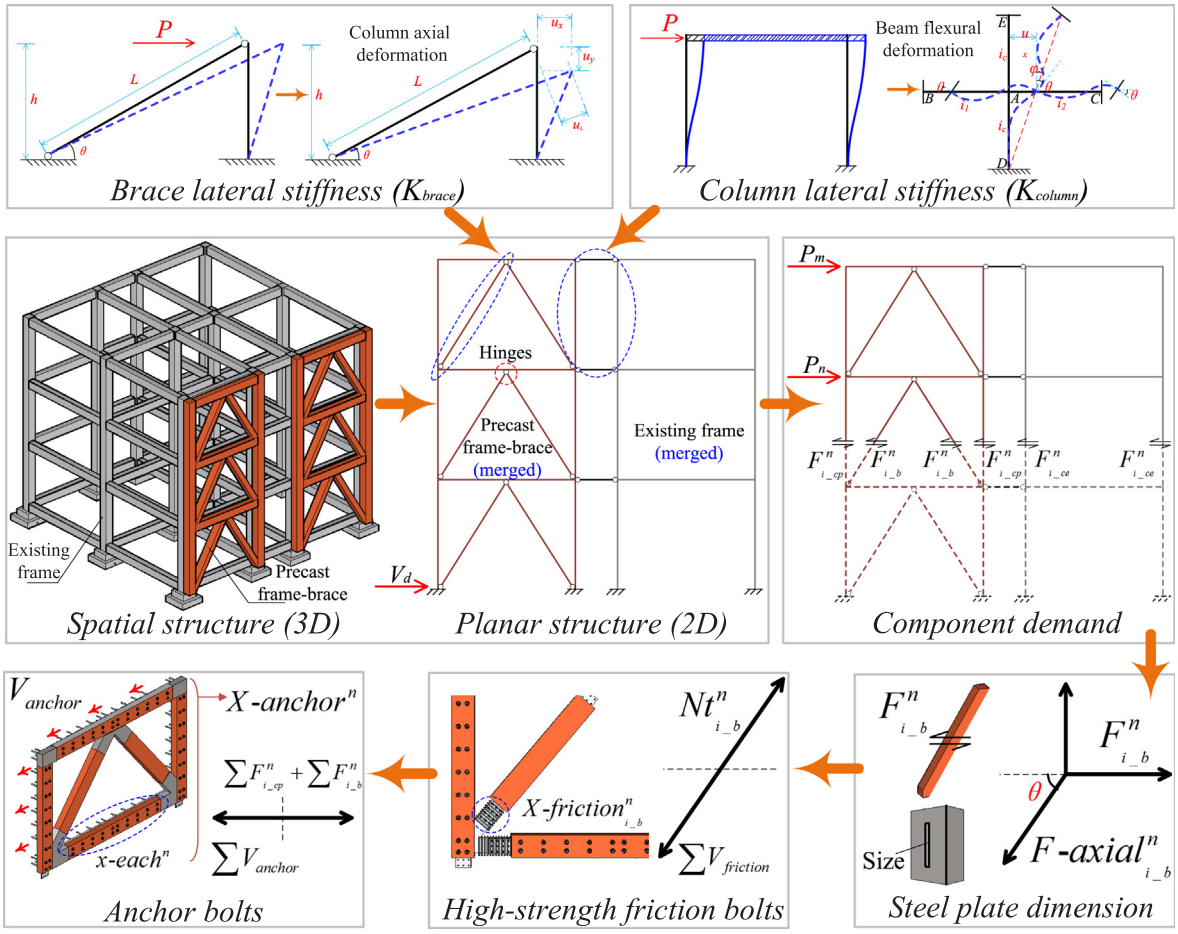

Fig. 10. Design procedure of PBSPC frame-brace sub-structure.

Step 6: The total lateral stiffness of storey n, K_n, is composed of three parts: (i) the stiffness of the existing RCF column, K_{ce}; (ii) the stiffness of the outside precast column, K_{cp}; and (iii) the stiffness of the outside precast brace, K_b. Eq. (7) presents the combination relationship, where $K^n_{i\_ce}$, $K^n_{i\_cp}$ and $K^n_{i\_b}$ represent the ith member on the nth floor for the existing RCF column, outside precast column and outside precast brace, respectively. At the same time, the total component numbers for the three parts on the nth floor are denoted as a_n, b_n and c_n. The coefficient η is introduced to consider the reduction effects of the assembly technology and correlation errors on the brace lateral stiffness. It is recommended to be 0.9 in this design procedure as the result of the mean values between the experimental data and numerical analysis, which is revealed in the following subsection.

$$K_n = \sum_{i=1}^{a_n} K^n_{i\_ce} + \sum_{i=1}^{b_n} K^n_{i\_cp} + \eta \sum_{i=1}^{c_n} K^n_{i\_b} \quad (n = 1, 2, \ldots, m) \tag{7}$$

The design shear demand of each member is then allocated based on its stiffness proportion, as expressed in Eq. (8).

$$\begin{aligned} F^n_{i\_ce} &= \frac{K^n_{i\_ce}}{K_n} \cdot \sum_{x=n}^{m} P_x \\ F^n_{i\_cp} &= \frac{K^n_{i\_cp}}{K_n} \cdot \sum_{x=n}^{m} P_x \\ F^n_{i\_b} &= \frac{K^n_{i\_b}}{K_n} \cdot \sum_{x=n}^{m} P_x \end{aligned} \tag{8}$$

where $F^n_{i\_ce}$, $F^n_{i\_cp}$ and $F^n_{i\_b}$ represent the design shear demand of the ith member on the nth floor for the existing RCF column, outside precast column and outside precast brace, respectively.

Step 7: As the precast brace is the main damage-bearing member and takes on more load due to its larger axial stiffness, the further component design is concentrated on it. Hinge connections are simplified at both ends because the brace itself contributes more to the lateral shear force compared with the moment. The relevant designs of the outside precast beam and column (e.g., steel plate dimensions and constructional reinforcement) are taken to have the same outcomes as the precast brace for the conservative consideration. To meet the force balance relationship, the following Eq. (9) is given:

$$F\_axial^n_{i\_b} = \frac{F^n_{i\_b}}{\cos\theta} \tag{9}$$

where $F\_axial^n_{i\_b}$ means the design axial demand of the ith brace on the nth floor.

Step 8: Because the tensile force of the brace is mainly undertaken by steel plates, only the tensile function of the steel plate is considered, and the tensile strength of the concrete is neglected. Thus, the tensile capacity of the brace, Nt, is calculated by the yield strength, f_y, and section area, A_s, of the steel plates. The compressive capacity of the brace, Nc, is limited as the stability bearing capacity under compression, for which the axial stability coefficient of the concrete members, φ, is adopted. Eq. (10) for Nt and Nc are expressed as follows:

$$\begin{aligned} Nt &= f_y A_s \\ Nc &= 0.9\varphi(f_{con} A_{con} + f_y A_s) \end{aligned} \tag{10}$$

During the design procedure, the design axial demand of the brace,

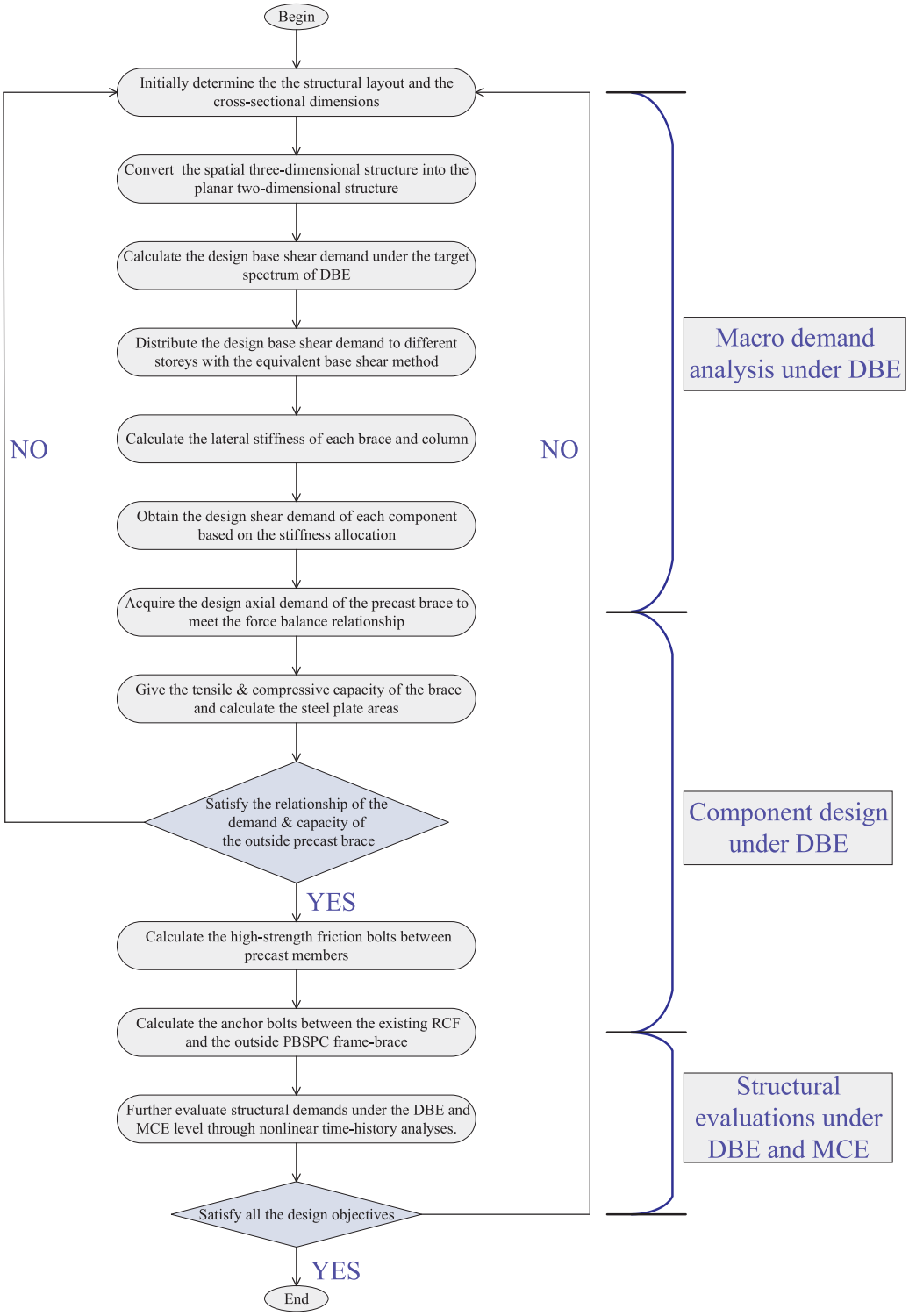

Fig. 11. Design flow chart of PBSPC frame-brace sub-structure.

$F\_axial_{i\_b}^{n}$, shall not exceed its tensile capacity, $Nt_{i\_b}^{n}$. Meanwhile, the tensile capacity, $Nt_{i\_b}^{n}$, shall not be larger than its compressive capacity, $Nc_{i\_b}^{n}$, so that the instability will not occur before the braces breakdown. The areas of the steel plates can be calculated afterwards based on the initially determined cross-sectional areas, and the relevant reinforcements such as constructional stirrups can also be determined [44]. The relationship between the demand and capacity is expressed as below. If the relationship cannot be achieved, the design procedure shall turn back to step 1 for a new section area estimation.

$$Nc_{i\_b}^{n} \geqslant Nt_{i\_b}^{n} \geqslant F\_axial_{i\_b}^{n} \quad (n = 1, 2, \ldots, m) \tag{11}$$

Step 9: The outside precast members are connected mutually by high-strength friction bolts, the shear capacity of which is denoted in Eq. (12)[40]. Since the brace is the main force-bearing member, the numbers of high-strength friction bolts are only calculated at the two ends of the brace. The connecting bolt numbers of the precast

Table 3
Component parameters of previous experimental tests conducted at Southeast University.

	Existing column	Existing beam	Precast column	Precast beam	Precast brace	
Section height (mm)	200	250	200	200	Section height (mm)	200
Section width (mm)	200	150	100	100	Section width (mm)	100
Moment of inertia ($\times 10^8$ mm^4)	1.333	1.953	0.667	0.667	Section area ($\times 10^4$ mm^2)	2
Axial length (mm)	1830	2700	1830	2700	Angle with the horizontal plane (°)	55
Line stiffness ($\times 10^9$ N·mm)	2.186	2.17	1.093	0.741	Line stiffness ($\times 10^5$ N/mm)	2.686
Beam-column stiffness ratio	0.9928		0.6778		Axial length (mm)	2234
Stiffness reduction factor α	0.4988		0.4398		Stiffness reduction factor λ	0.3547
Modified lateral stiffness ($\times 10^4$ N/mm)	0.391	N/A	0.172	N/A	Modified lateral stiffness ($\times 10^4$ N/mm)	5.7

Note: Line stiffnesses for column & beam and brace are calculated as EI/L and EA/L, respectively.

beam and column are the same as those of the brace for the conservative consideration.

$$V_{friction} = 0.9 n_f \mu T_p \tag{12}$$

To make full use of the tensile properties of the built-in steel plate and make sure that premature damage does not occur at the connection joints, the shear capacities provided by all the high-strength friction bolts at each joint shall exceed the tensile capacity of the brace. The number of high-strength friction bolts is presented by Eq. (13).

$$X\_friction^n_{i\_b} \geqslant \frac{Nt^n_{i\_b}}{V_{friction}} \quad (n = 1, 2, ..., m) \tag{13}$$

where $X\_friction^n_{i\_b}$ is the total number of high-strength friction bolts at each end of the ith brace on the nth floor.

Step 10: The anchor bolts between the existing RCF and outside PBSPC frame-brace are the main connectors to transfer shear strength and make sure that the whole structures work together under hazards. The shear capacity of the anchor bolt, V_{anchor}, is expressed as the minimum value of V_s and V_c, where V_s represents the shear capacity of the steel components, while V_c represents the shear capacity of the substrate concrete that the anchor bolts penetrate through [45]. Eq. (14) is shown as follows:

$$\begin{aligned} V_{anchor} &= \min[V_s, V_c] \\ V_s &= \psi_s f_y A_e \\ V_c &= 0.4\sqrt{E_{con} f_{con}}\, A_e \end{aligned} \tag{14}$$

The anchor bolt number of each component on the nth floor, x_each^n, is estimated as the ratio between the brace horizontal tensile capacity and anchor bolt shear capacity, as shown in Eq. (15). In view of the inverted V shape substructure form, two precast braces are bound in a group with one in the tensile state and the other in the compressive state. Thus, an amplification factor of 2 is considered.

$$x\_each^n \geqslant \frac{2Nt^n_{i\_b}\cos\theta}{V_{anchor}} \quad (n = 1, 2, ..., m) \tag{15}$$

For all of the anchor bolts of the nth floor, X_anchor^n, the number considers all the shear demands of the outside precast columns and braces of the nth floor. The force balance and moment balance conditions are as follows.

$$\begin{aligned} &X\_anchor^n \geqslant \frac{\sum_{i=1}^{b_n} F^n_{i\_cp} + \sum_{i=1}^{c_n} F^n_{i\_b}}{V_{anchor}} \quad (n = 1, 2, ..., m) \\ &V_{anchor} \cdot \sum_{i=1}^{X\_anchor^n} h_i^n \geqslant \Big(\sum_{i=1}^{b_n} F^n_{i\_cp} + \sum_{i=1}^{c_n} F^n_{i\_b}\Big) \cdot H_n \quad (n = 1, 2, ..., m) \end{aligned} \tag{16}$$

where h_i^n represents the height from the centre of the ith anchor bolt to the nth floor. Generally, anchor bolts are not allowed to be destroyed during earthquakes, and so they are designed in an elastic state. For assurance, the calculated basic numbers shall be properly enlarged and evenly arranged. Appropriate enhancements in the joint zones are needed.

Step 11: The structural demands (i.e., maximum inter-storey drift ratios, maximum inter-storey shear forces and top displacement variations) are further evaluated under the DBE and MCE level through nonlinear time-history analyses. If any of the calculated structural responses are significantly smaller than the allowable thresholds or if the demands exceed the allowable thresholds, the layout and dimensions of the outside PBSPC frame-brace may need to be revised, and the design procedure shall turn back to step 1 for a new section area estimation.

A design flow chart that summarizes the procedure is shown in Fig. 11.

4.3. Determination of coefficient η

During the design shear demand allocation of the procedure, the coefficient η is introduced to consider the reduction effect on the brace lateral stiffness because there exist assembly errors and initial defects. The coefficient η is determined using both the experimental and simulation methods. The final recommended value is taken as the average of the two methods. According to the previous experimental tests conducted at Southeast University, the relevant component parameters and the modified lateral stiffness for the existing column, the precast column and the precast brace are shown in Table 3 based on the aforementioned Eqs. (3) and (4).

For the experimental method, the load-displacement curve is adopted, the initial hysteresis loop is marked in red (Fig. 12(a)), and the structure is regarded to be in the elastic state. The peak points of the initial hysteresis loop are selected, and the initial elastic stiffness is calculated as the slope of the two points. The initial elastic stiffness is theoretically equal to the sum of the component lateral stiffnesses, as denoted in Eq. (17). The coefficient η_1 from the experimental method is determined to be 0.8686.

$$\begin{aligned} K_{initial} &= K_{ce} \times 2 + K_{cp} \times 2 + (K_{bt} + K_{bc}) \times \eta_1 \\ 110.283 \times 10^3 &= (0.391 + 0.172 + 5.70 \times \eta_1) \times 10^4 \times 2 \\ \eta_1 &= 0.8686 \end{aligned} \tag{17}$$

For the simulation method, the relationship between the brace horizontal force and the external load is adopted (Fig. 12(b)). The blue line represents the tensile brace, while the red line represents the compressive brace. The relationship is linear in the initial stage because the components are in the elastic state, during which time the initial stiffness is used. Two points are chosen from the initial stage to calculate the slope with the origin point. The sum of the two slopes is theoretically equal to the ratio of the brace stiffness to the whole storey stiffness, as denoted in Eq. (18). The coefficient η_2 from the simulation method is determined to be 0.9144.

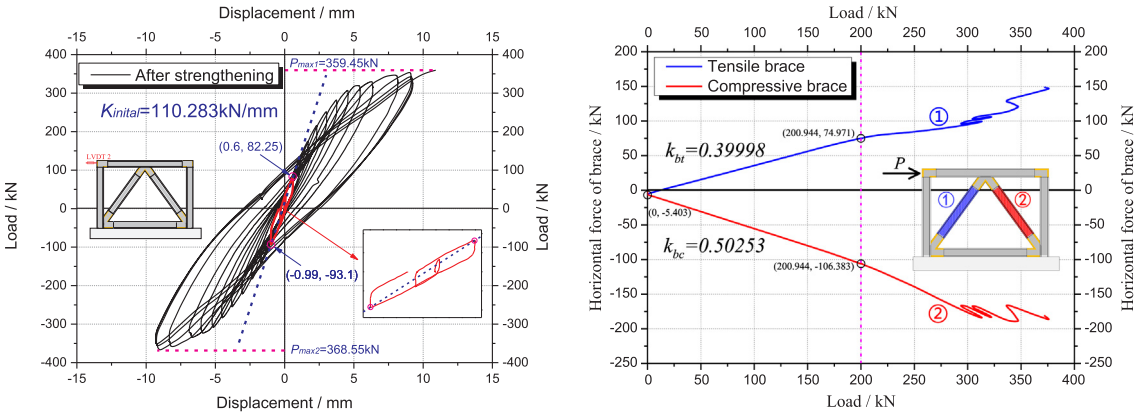

(a) Experimental method (b) Simulation method

Fig. 12. Determination of coefficient η.

$$k_{bt} + k_{bc} = \frac{F_{btx} + F_{bcx}}{P} = \frac{K_b}{K_{initial}} = \frac{(K_{bt} + K_{bc}) \times \eta_2}{(K_{bt} + K_{bc}) \times \eta_2 + (K_{ce} + K_{cp}) \times 2}$$

$$0.39988 + 0.50253 = \frac{5.70 \times 10^4 \times 2 \times \eta_2}{5.70 \times 10^4 \times 2 \times \eta_2 + (0.391 + 0.172) \times 10^4 \times 2}$$

$$\eta_2 = 0.9144 \tag{18}$$

The final recommended parameter for the design procedure, η, is taken as the average of the experimental value, η_1, and the simulation value, η_2, which approximates to 0.9, as presented in Eq. (19).

$$\eta = \frac{\eta_1 + \eta_2}{2} = \frac{0.8686 + 0.9144}{2} = 0.8915 \approx 0.9 \tag{19}$$

5. Case study

5.1. Building description

The proposed outside PBSPC frame-brace strengthening substructures were applied in the seismic performance upgrade of a five-storey RC frame building located in Huhhot, China, with a seismic fortification intensity of eight degrees. The corresponding design peak ground acceleration (PGA) is 0.2 g, which indicates a 10% probability of exceedance in 50 years considering the earthquake impact [39].

The function of the building was adjusted from an office building to a hospital, and the seismic level of the original frame was improved from II to I, which means an internal force modification and reinforcement recalculation, and as a result, the beams and columns need to be strengthened [39]. The original structural layout is irregular, with dimensions of 104 m × 45.5 m and a total height of 20 m (storey height of 4 m), as shown in Fig. 13(a). The building is located on a class-II site (with a cover thickness over 5 m and an equivalent shear wave velocity between 250 m/s and 500 m/s) [39]. The structural stiffness in the longitudinal direction is obviously stronger than that in the transverse direction, and thus a 3-span frame on the side of the transverse direction (with a span length of 5.5 m) was selected to verify the upgrade effectiveness of the PBSPC frame-brace (Fig. 13(b)).

The cross section of both the original column and beam is 500 mm × 500 mm. For the beam, four longitudinal rebars are set at the top of the section, with 2 of 32 mm diameter on the outside and 2 of 25 mm diameter on the inside. Four longitudinal rebars of 25 mm diameter are set at the bottom. In the section middle, two constructional rebars of 10 mm diameter are placed, between which tie rebars of 8 diameters were used at a spacing of 500 mm. For the column, four longitudinal rebars of 32 mm diameter are laid at both the top and the bottom of the section. Four constructional rebars of 10 mm diameter are arranged evenly in the middle, as shown in Fig. 13(c). For both the beam and column, the stirrups of 8 mm diameter are placed at a spacing of 100 mm near the joint core (1000 mm from the connection surface), and the interval changes to 200 mm outside the zones. According to the initial design of the building, the nominal yield strength for the longitudinal rebars is 335 MPa, with the symbol of HRB335, whereas the nominal yield strength for the stirrups and the tie rebars is 300 MPa, with the symbol of HPB300. The compressive strength of the concrete is regarded as 30 MPa.

5.2. Seismic upgrade

The seismic upgrade using the outside PBSPC frame-braces was based on the aforementioned design procedure, and for the selected 3-span-5-storey frame to be strengthened, the layout of the outside substructures was preliminarily determined as an inverted V-shape along the total height, arranged only in the middle span (Fig. 13(b)). The 3D-spatial structure was then converted to a 2D-planar structure, with four existing RCF columns, two precast columns and two precast braces for each storey. The cross section of the precast brace was given as 250 mm × 500 mm for the trial calculation, after which the components' shear demand was acquired in view of the EBSP and stiffness allocation under the DBE (with the corresponding spectral acceleration-period relationship for 0.2 g PGA). The concrete compressive strength of the outside substructure was the same as that of the original structure (30 MPa). The nominal yield strength of the steel plate was adopted as 345 MPa, and its cross section was obtained as 15 mm × 300 mm according to the tensile capacity and axial demand relationship (Eq. (11)). Four auxiliary rebars with a diameter of 10 mm were placed at the four corners, and the constructional stirrups with a diameter of 8 mm were set at a spacing of 100 mm. Both the auxiliary rebars and constructional stirrups were made of HRB335 steel. The axial stability coefficient of the outside brace was calculated as 0.895 (with an axial length of 3832 mm and section width of 250 mm) [43]. The tensile and compressive capacities of the outside brace were calculated and came to 1553 kN and 4162 kN, respectively, satisfying the capacity requirements (Eqs. (10) and (11)). The structural responses evaluations after strengthening will be proven by time-history analyses in a later subsection.

The high-strength friction bolts were selected as M20-10.9, which represents a nominal diameter of 20 mm, nominal ultimate strength of 1000 MPa and ratio between the yield strength and ultimate strength of 0.9. The shear capacity of each high-strength friction bolt was calculated as 139.5 kN (with an anti-slip coefficient of 0.5, pre-tension force of 155 kN and 2 friction surfaces) [43]. The total friction bolt number at each end of the brace was given as 12, so the whole shear capacity provided by the friction bolts was 1674 kN, larger than the tensile capacity of the brace (1553 kN). The bolt number at the end of the precast beam and column was also 12, consistent with the brace, as displayed in Fig. 13(d) and (e).

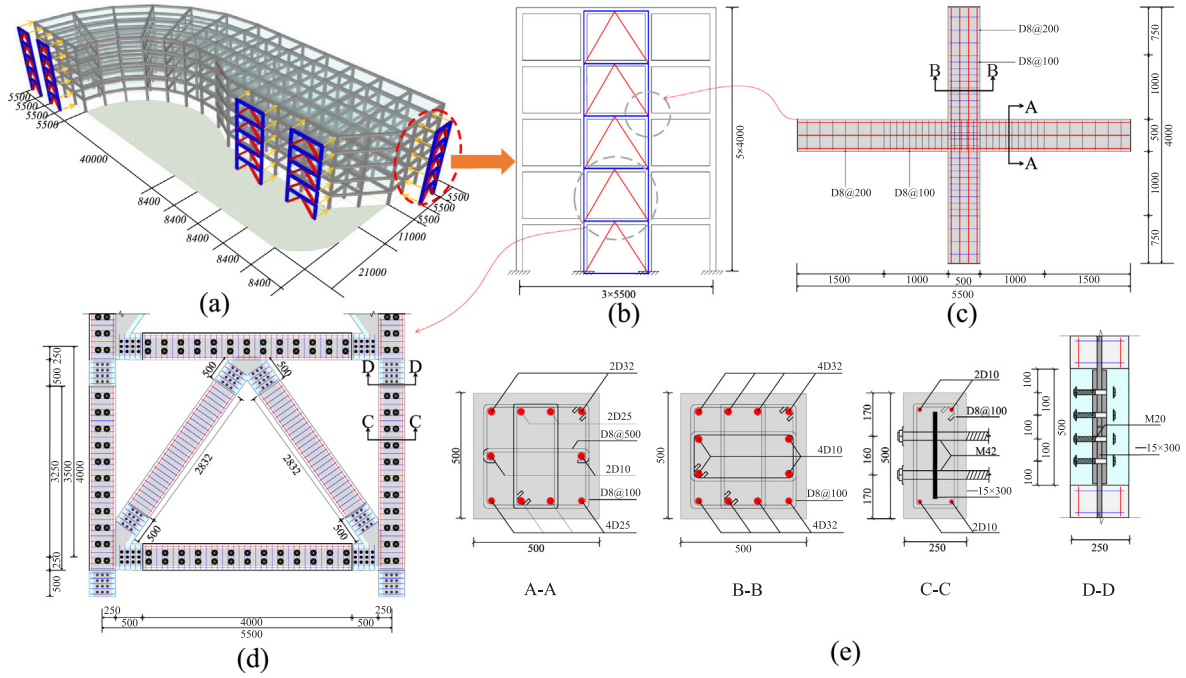

Fig. 13. Case study: (a) dimensions of the original building; (b) a 3-span frame on the side of the transverse direction; (c) joint of the existing RCF; (d) dimensions of the outside PBSPC frame-brace after design; (e) cross areas of different sections.

The anchor bolts between the existing RCF and outside PBSPC frame-brace were selected as M42-10.9, and the shear capacity for each one was adopted as 271 kN (with a seismic reduction coefficient of 0.7, steel plate yield strength of 345 MPa and effective section area of 1121 mm^2) [45]. The basic calculated number for each component is 7 (Eq. (15)), whereas the actual numbers for each precast column and beam came to 22 and 26, respectively (Fig. 13(d) and (e)), which tripled to confirm the combination. The force and moment balance requirements were consequently satisfied. The spacing of all the friction bolts and anchor bolts shall exceed the minimum limitations [43].

5.3. Selection of ground motions

To evaluate the upgrade effect of the PBSPC frame-brace substructure, 22 far-field ground motion records recommended by FEMA P-695 [46] were used as excitations for the nonlinear time-history analyses. Table 4 shows the characteristics of the 22 earthquake waves. Each ground motion record is selected from the PEER Strong Motion Database, and then its amplitude is modulated to statistically fit the DBE and MCE level spectra, using the adjusting function of the Database (Fig. 14). The disparities between the target spectrum and the average spectrum after adjustment are less than 20% at the major considered frequencies [39].

5.4. Seismic responses

The structural demands are further evaluated from the maximum inter-storey drift ratios, maximum inter-storey shear forces and top displacement variations. Nonlinear time-history analyses were conducted under the DBE and MCE levels based on the 22 modified earthquake ground motions using the numerical methods put forward in this paper.

The maximum inter-storey drift ratios before and after strengthening are displayed in Fig. 15(a) and (b). The red lines represent the threshold values, which are equal to 0.5% and 1% for the DBE and MCE levels, respectively, in accordance with the design objectives. The dotted-grey lines represent the seismic responses of the 22 earthquake waves before strengthening, while the solid grey lines show the results after strengthening. The black, blue and pink lines indicate the mean values (μ), mean values minus standard deviations ($\mu - \sigma$) and mean values plus standard deviations ($\mu + \sigma$), respectively.

It can be observed that under the DBE level, the maximum inter-storey drift ratios of the second and third floors exceed the threshold value before strengthening. The mean values (μ_1) are equal to 0.507%, 0.747%, 0.663%, 0.573% and 0.423% from the first to fifth floor, among which the values of the second and third floors are approximately 1.49 and 1.33 times that of the threshold value. In contrast, the maximum inter-storey drift ratios are all below the thresholds after strengthening. The mean values (μ_2) drop to 0.207%, 0.218%, 0.204%, 0.179% and 0.106%, which are more uniform along the structure height. The discreteness of the results before strengthening is obvious, especially on the fourth floor with a larger standard deviations (σ_1), whereas the data (σ_2) decreased after strengthening.

The same phenomenon happened when subjected to the MCE level earthquake waves. Most of the inter-storey drift ratios before strengthening exceeded the thresholds as well, centred on the second, third and fourth floors. The mean values reached 1.40%, 1.82%, 1.65%, 1.59% and 1.02% from the first to fifth floor, accompanied by the maximum value of 2.72% on the fourth floor for the ground motion NO.15-ABBAR-T, almost 1.82 times that of the threshold value. However, the mean values decreased to 0.652%, 0.659%, 0.623%, 0.569% and 0.368% after strengthening, satisfying the threshold requirements. In addition, the deformation patterns become uniform with a lower discreteness, avoiding the soft storey effect, and the standard deviations (σ_2) of all the storeys apparently shrank according to the blue and pink lines.

The maximum inter-storey drift ratios of each earthquake wave are displayed in Fig. 15(c) and (d), showing that all the maximum responses under the DBE and MCE levels are beyond the thresholds before upgrading. However, the results decreased under the limitations after upgrading, indicating that the outside PBSPC frame-brace substructures provide an additional lateral stiffness, changed the deformation patterns and upgraded on the structural-system level.

Fig. 16(a) and (b) illustrate the maximum inter-storey shear force at the bottom of the side column in the existing RCF under the DBE and MCE levels, respectively. The colour symbols are the same as those in

Table 4
Seismic records Selected for analysis.

Number	Name	Year	Component	Moment Magnitude	PGA (g)	Duration (s)
1	Northridge	1994	MUL279	6.7	0.52	30
2	Northridge	1994	LOS270	6.7	0.48	20
3	Duzce	1999	BOL090	7.1	0.82	55.9
4	Hector Mine	1999	HEC090	7.1	0.34	45.3
5	Imperial Valley	1979	H-DLT352	6.5	0.35	99.9
6	Imperial Valley	1979	H-E11230	6.5	0.38	39
7	Kobe	1995	NIS090	6.9	0.51	41
8	Kobe	1995	SHI090	6.9	0.24	41
9	Kocaeli	1999	DZC270	7.5	0.36	27.2
10	Kocaeli	1999	ARC090	7.5	0.22	30
11	Landers	1992	YER360	7.3	0.24	44
12	Landers	1992	CLW-TR	7.3	0.42	28
13	Loma Prieta	1989	CAP090	6.9	0.53	40
14	Loma Prieta	1989	G03090	6.9	0.56	40
15	Manji	1990	ABBAR-T	7.4	0.51	46
16	Superstition Hills	1987	B-ICC090	6.5	0.36	40
17	Superstition Hills	1987	B-POE360	6.5	0.45	22.3
18	Cape Mendocino	1992	RIO360	7	0.55	36
19	Chi-Chi	1999	CHY101-N	7.6	0.44	90
20	Chi-Chi	1999	TCU045-N	7.6	0.51	90
21	San Fernando	1971	PEL180	6.6	0.21	28
22	Friuli	1976	A-TMZ270	6.5	0.35	36.3

the inter-storey drift ratios. It can be seen that the shear force of the existing RCF decreased obviously, relieving the seismic demands of the original column. Generally the maximum shear force happened on the first floor for both conditions. Under the DBE level, the mean shear force (μ) of the first floor shifted from 148.7 kN to 91.2 kN after upgrading, a 38.7% drop. The maximum declining value of the mean shear force occurred on the second floor, to approximately 66.1 kN. Under the MCE level, the mean shear force (μ) of the first floor shifted from 413.1 kN to 307.2 kN after upgrading, a drop of 25.6%. The maximum declining value of the mean shear force occurred on the top floor, reaching up to 210.3 kN. The shear force discreteness of all the storeys also decreased with a smaller deviation (σ) for both the DBE and MCE.

Fig. 16(c) and (d) show the maximum inter-storey shear force of each earthquake wave before and after upgrading. The changes in the maximum inter-storey shear force indicates that the PBSPC frame-brace works together with the existing structure under the earthquake and alters the force-transferring mechanisms. The precast brace undertakes significantly more load due to its larger stiffness and thus protects the original structure.

The top displacement-time history curves of the earthquake ground motions NO.7-NIS090, NO. 10-ARC090, NO. 14-G03090, NO. 17-B-POE360 and NO. 21-PEL180 are displayed from Fig. 17(a)–(e). Each figure is composed of two parts, with the upper half showing the DBE results and the lower half showing the MCE results. According to the DBE responses, the maximum top displacements of all the five waves are lowered in general, especially at the time of the original peak points. The reduced values range from 30.0 mm to 58.7 mm. The gaps between the two peak displacements before and after strengthening reach up to 40.1 mm, 15.1 mm, 27.0 mm, 31.8 mm and 24.9 mm, respectively, for the five waves.

With regard to the responses under the MCE level, residual displacements appeared in the structures without strengthening, which attained 85.1 mm and 106.6 mm under NO. 14-G03090 and NO. 21-PEL180, whereas the values dropped to 1.41 mm and 2.89 mm, respectively, after strengthening. The largest residual displacement of the five waves occurred under NO. 10-ARC090, as high as 209.0 mm, which declined to 1.61 mm after upgrading, showing the effectiveness of the outside substructure.

Compared with the un-strengthened structure, the maximum top displacements also dropped greatly, with gaps ranging from 86.0 mm to 165.3 mm for the five waves, which mainly results from the great stiffness provided by the additional braces.

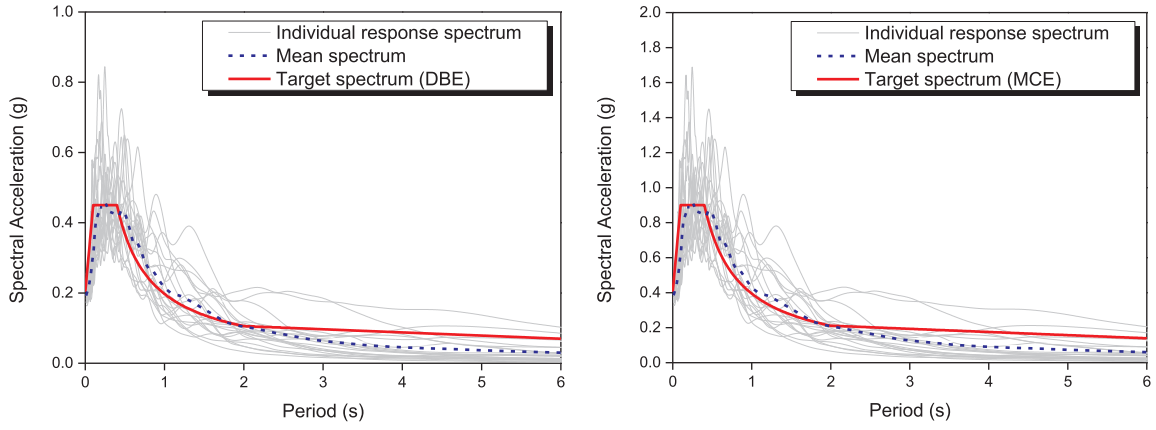

(a) DBE level (b) MCE level

Fig. 14. Selection of ground motions.

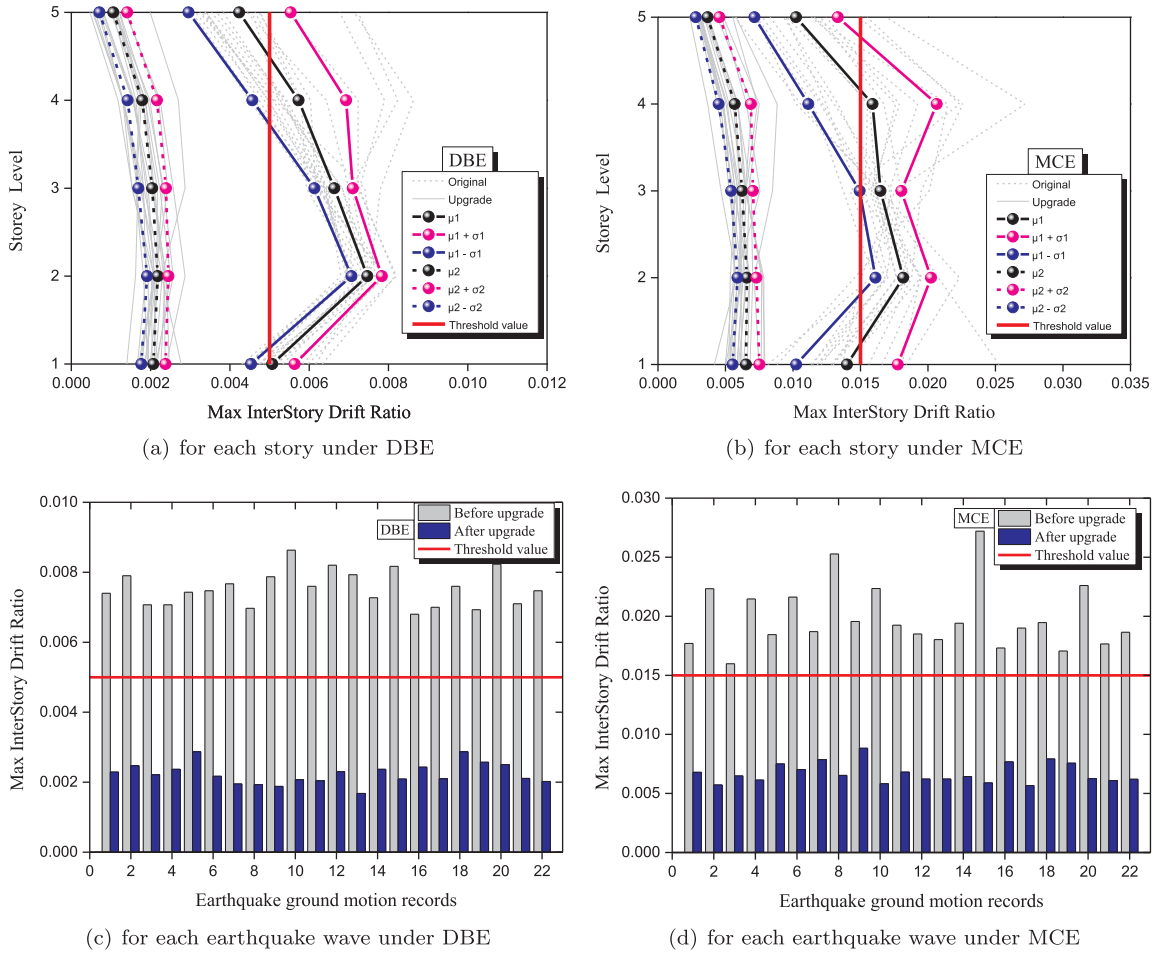

(a) for each story under DBE

(b) for each story under MCE

(c) for each earthquake wave under DBE

(d) for each earthquake wave under MCE

Fig. 15. Maximum interstory drift ratio.

5.5. Incremental Dynamic Analysis (IDA)

Incremental dynamic analysis (IDA) is a promising parametric analysis method developed in recent years to comprehensively evaluate the structural performance under ground motions. IDA curves reflect the entire response history of a structural system from the linear elastic state to the overall collapse state under increasing intensity levels, providing complete seismic demands and performance assessments.

In this study, the 22 earthquake ground motions mentioned before were used to conduct the IDA and investigate the structural performance after strengthening. The spectral acceleration of the first mode ($S_a(T_1)$) was selected as the intensity measure (IM) to reflect intensity variations, which is proven to be efficient and proficient for its smaller dispersion and better correlation compared with the PGA [47]. The maximum interstory drift ratio (θ_{max}) and the maximum residual interstory drift ratio ($\theta_{r,max}$) were chosen as the engineering demand parameters (EDP) to represent the structural responses against the earthquake records. Through a series of scale factors, each earthquake wave is extended to a few waves, and then time-history analyses were performed sequentially, with $S_a(T_1)$ changing from 0 to 3.0 g at an interval of 0.1 g. The structure can be regarded as collapsed when the IDA curve becomes a horizontal line (lower than the 20% of the initial slope), accompanied by a tremendous increment in the EDP and non-convergence in numerical computations.

The IDA consequences of all 22 earthquake motions are demonstrated with grey lines for the un-strengthened frame (Fig. 18)) and the one strengthened with outside PBSPC frame-brace substructures (Fig. 18(b) and (d)). Three performance levels and the corresponding control objectives recommended by FEMA 356 [38] are adopted for further evaluations. In addition to the immediate occupancy (IO) and life safety (LS) targets mentioned in the design procedure, the collapse prevention (CP) level is also captured, which represents the verge of partial or total collapse with huge severity. The maximum transient interstory drift ratios (θ_{max}) for the IO, LS and CP performance levels are defined as 0.5%, 1.5% and 4%, and the maximum residual interstory drift ratios ($\theta_{r,max}$) for the IO, LS and CP performance levels are defined as 0.1%, 0.5% and 1%. The three vertical lines representing the IO, LS and CP are illustrated with purple lines in Fig. 18.

To statistically deal with the IDA curves and quantitatively analyse the multiple IDA data, the fractile IDA curves of 16%, 50%, and 84% appear as red, pink and blue lines respectively in Fig. 18. The calculations are based on the assumption that both the IM and EDP shall fulfil lognormal distributions [47]. The required $S_a(T_1)$ values to reach the three performance levels (θ_{max} = 0.5%, 1.5%, 4% and $\theta_{r,max}$ = 0.1%, 0.5%, 1%) are depicted from the three fractile IDA curves, and the statistics are summarized in Table 5, before and after upgrading.

It can be observed that under the same θ_{max}, the $S_a(T_1)$ needed improves greatly. Taking the 50% fractile curve, for example, the corresponding $S_a(T_1)$ for the θ_{max} of 0.5% (IO) is 0.1 g before strengthening, which means that half of the earthquake waves shall possess an $S_a(T_1)$ over 0.1 g to get the θ_{max} of 0.5%. However, the required $S_a(T_1)$ increased significantly to 0.3 g after strengthening, three times the original value. The $S_a(T_1)$ for the θ_{max} of 1.5% (LS) and 4.0% (CP) improved as well, from 0.28 g to 0.75 g and 0.78 g to 1.27 g, respectively, showing the effectiveness of the strengthening method. Similar conditions occurred for the EDP of $\theta_{r,max}$. In other words, under the same $S_a(T_1)$, the required θ_{max} or $\theta_{r,max}$ of all three fractile curves decreased after strengthening, making it harder to exceed the limitations of the

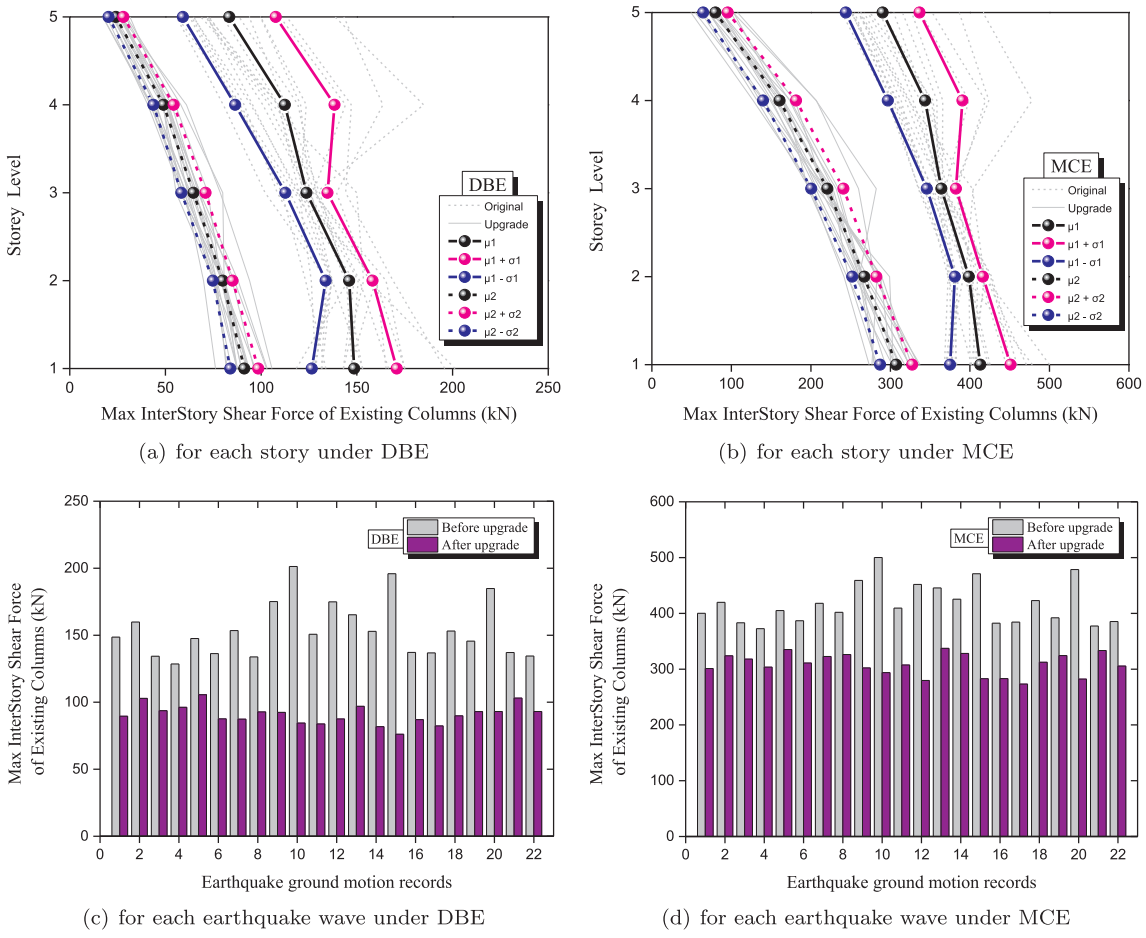

(a) for each story under DBE

(b) for each story under MCE

(c) for each earthquake wave under DBE

(d) for each earthquake wave under MCE

Fig. 16. Maximum interstory shear force.

performance levels and safer by guaranteeing the structural capacities.

5.6. Seismic fragility analysis

This section provides an assessment of the seismic vulnerability by developing fragility curves for the existing RCF before and after strengthening. It refers to the possibility of the structure reaching or exceeding a certain limit state or damage degree under seismic excitations with different intensities. In general, the fragility analysis is based on the IDA results and defined as the conditional probability for a given IM.

As shown in Fig. 19, a linear regression of the log-transformed IM-EDP pairs is performed (red lines), after which the relevant parameters such as the slope, intercept, demand median and standard deviation can be given for the fragility calculation (EDP of θ_{max}). The blue lines denote the boundary values of the regression considering the dispersion. In view of the hypothesis that both the structural capacity (C) and seismic demand (D) shall satisfy lognormal distributions, the functions to generate the fragility curves are defined as:

$$P[D > C|IM] = \Phi\left[\frac{\ln(S_d/S_c)}{\sqrt{\beta_d^2 + \beta_c^2 + \beta_m^2}}\right] \tag{20}$$

where S_d represents the median structural demand, which can be acquired from the aforementioned IM-EDP linear regression, conditioned on each IM. S_c represents the median structural capacity, which is in accordance with the performance levels (IO, LS, CP) as well as the corresponding θ_{max} (0.5%, 1.5%, 4%). β_d, β_c and β_m indicate the uncertainties of the structural demand, capacity and modelling, respectively, among which β_c and β_m are often assumed to range from 0.2 to 0.47 [48,49] (taken as 0.2 in this paper) while β_d is taken to be the logarithmic standard deviation obtained from the IM-EDP linear regression (shown in Fig. 19). $\Phi[\cdot]$ is the standard normal distribution function.

Fig. 20 displays the resulting fragility curves for the existing RCF before and after strengthening (EDP of θ_{max}). The blue, green and red lines represent the performance levels of IO, LS and CP, respectively. The solid lines denote the conditions before upgrading, while the dotted lines denote those after upgrading. Generally, the fragility curve for each performance level moves significantly towards the right, meaning that under the same $S_a(T_1)$, the exceeding probability of the corresponding θ_{max} dropped sharply. Based on the first period of the structure (T_1) before and after strengthening, the corresponding target $S_a(T_1)$ under both the DBE and MCE levels (red lines in Fig. 14) are calculated and depicted as vertical lines, as shown in Fig. 20. The intersections between the fragility curves and the vertical lines are reflected in Table 6.

It can be observed that the decline in the exceeding probability is so significant that it can make up for the increment in $S_a(T_1)$ for both earthquake levels. The largest dropping percentage for the IO and LS levels reached as high as 47.7%, from 85.6% to 37.9% (IO level under DBE), and the structural collapse will not happen after strengthening (0% exceedance for the CP level both under DBE and MCE). The median values (50%) are equal to 0.09 g, 0.30 g and 0.86 g for the IO, LS and CP levels before strengthening, whereas the values improved to 0.24 g, 0.61 g and 1.37 g after strengthening, respectively, showing the greater reliability in the structural capacity and the less possibility of structural damage after strengthening.

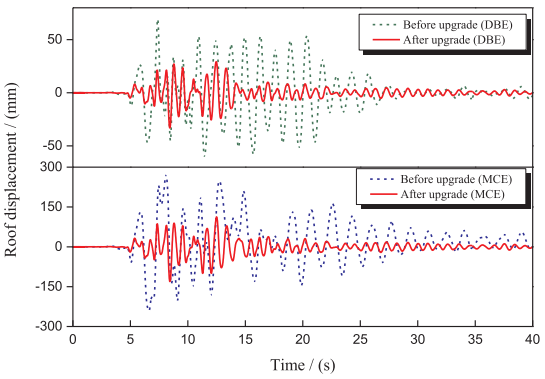

(a) NO.7-NIS090

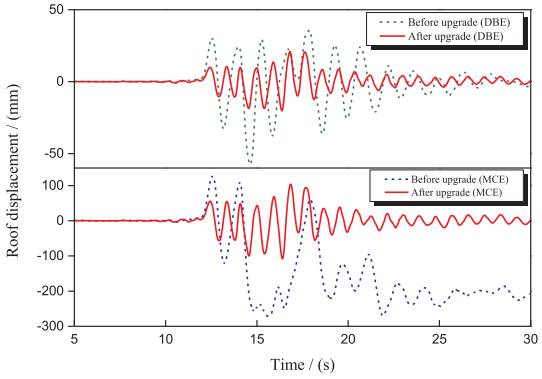

(b) NO. 10-ARC090

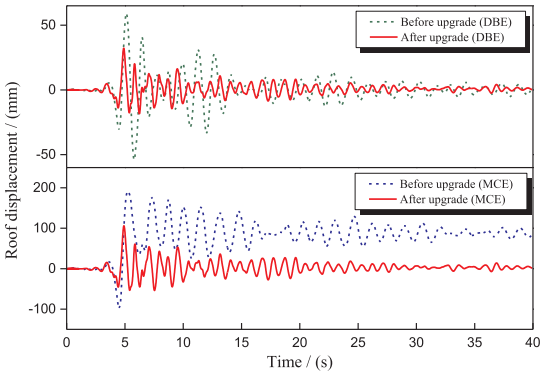

(c) NO. 14-G03090

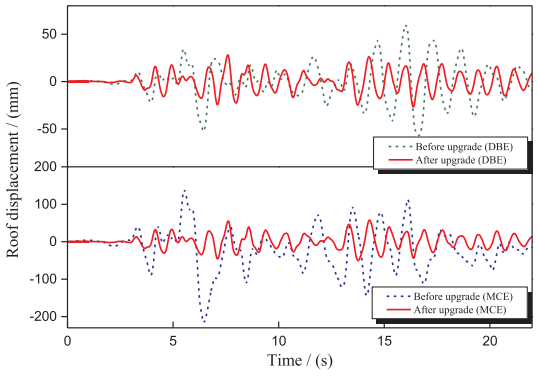

(d) NO. 17-B-POE360

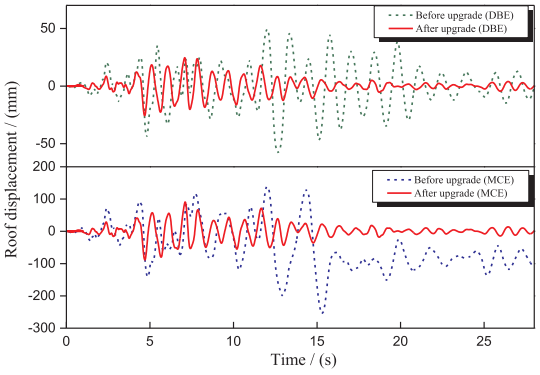

(e) NO. 21-PEL180

Fig. 17. Top displacement-time history curves.

6. Conclusions

This paper introduces a new strengthening method for an existing frame by an outside substructure, namely, the precast bolt connected steel plate reinforced concrete (PBSPC) frame-brace. The working principles, numerical methods, design procedures and case studies of the upgrading system were presented, from which the following conclusions may be drawn:

(1) The PBSPC frame-braces work together with the existing RCF and improve the overall performance on a structural-system level by altering the force transferring mechanisms and deformation modes. The prefabrication process and assembly technology ensure the component quality while reducing the strengthening period. The sub-structure strengthens the existing beam and column simultaneously and provides a place for additional braces, which effectively prevents the condition that the joints of the existing RCF damage earlier.

(2) A 3D numerical model is proposed to reflect the characteristics of the upgrading sub-structure. The Joint3D element as well as Pinching4 material were adopted to consider the influences of beam-column joint zones. The zerolength element as well as hysteretic material model were used to analyse the effects of beam-brace joint zones. The proposed simulation method was validated by experiments conducted previously, and the results showed satisfactory consistency, indicating the effectiveness of the numeric model.

(3) A stiffness-based design procedure for the upgrading system was put forward, generally composed of 3 parts, including macro demand analysis, component design and structural evaluations. The

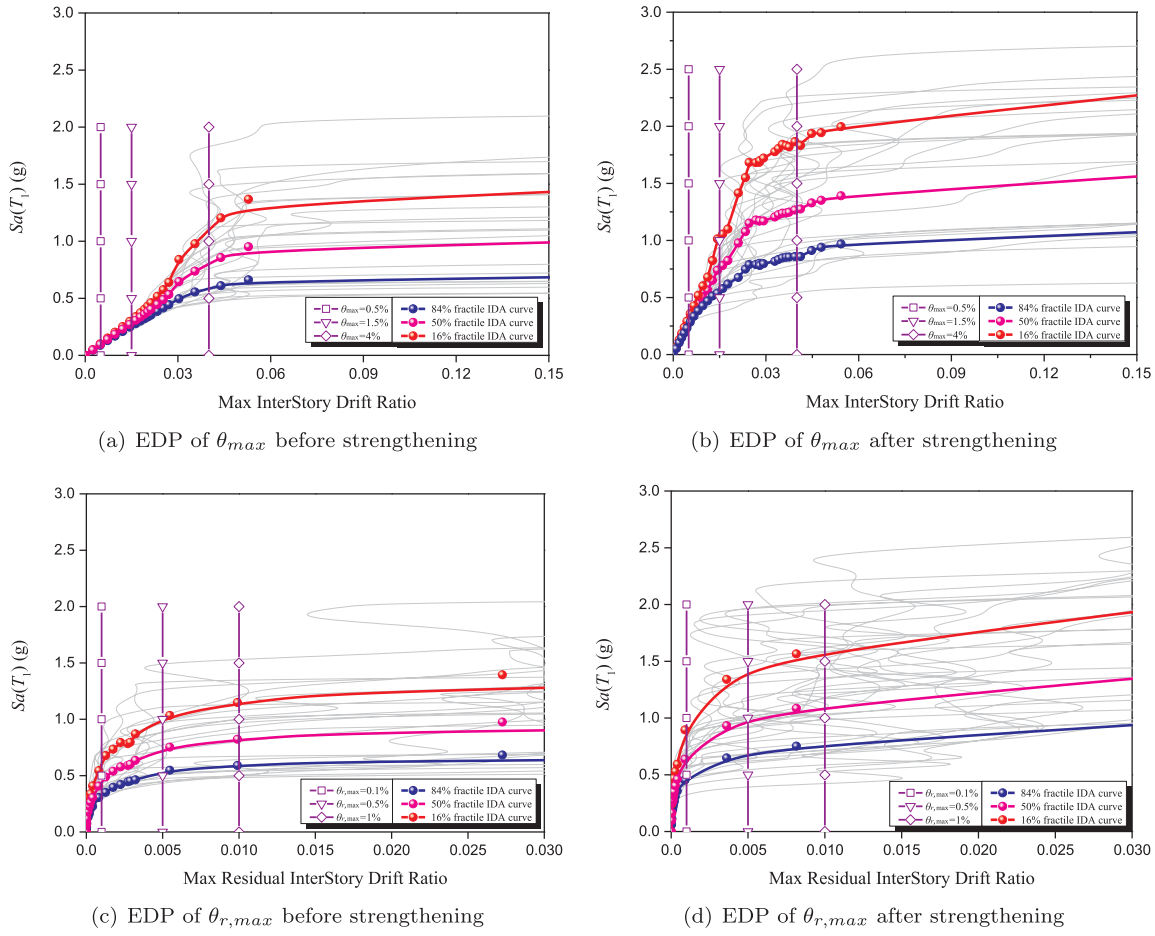

(a) EDP of θ_{max} before strengthening

(b) EDP of θ_{max} after strengthening

(c) EDP of $\theta_{r,max}$ before strengthening

(d) EDP of $\theta_{r,max}$ after strengthening

Fig. 18. 22 IDA curves and 3 fractile curves.

Table 5
The required $S_a(T_1)$ to reach the three performance levels from the fractile IDA curves.

	Before upgrade			After upgrade		
	16%	50%	84%	16%	50%	84%
θ_{max} = 0.5%	0.12	0.1	0.08	0.33	0.3	0.26
θ_{max} = 1.5%	0.31	0.28	0.25	1.03	0.75	0.56
θ_{max} = 4%	1.11	0.78	0.57	1.85	1.27	0.86
$\theta_{r,max}$ = 0.1%	0.60	0.44	0.32	0.84	0.61	0.45
$\theta_{r,max}$ = 0.5%	0.98	0.72	0.52	1.38	0.97	0.67
$\theta_{r,max}$ = 1%	1.13	0.82	0.58	1.56	1.09	0.75

design base shear demand, each story's shear demand, and the modified lateral stiffness were calculated, and each component's shear demand was allocated accordingly. The component design was concentrated on the precast braces as the main damage-bearing members, within which the high-strength friction bolts and anchor bolts were further analysed. The coefficient η that considers the precast influences was recommended to be 0.9.

(4) A practical engineering project was studied based on the proposed numerical model and design process. The seismic responses were further evaluated under the DBE and MCE. The maximum interstory drift ratios significantly decreased within the thresholds, and the maximum interstory shear force of the existing RCF decreased, showing that the inner force transferred to the external sub-structure. The top displacements dropped significantly, especially for the residual displacements under the MCE. The IDA curves and the fragility curves were plotted, illustrating the greater reliability in the structural capacity and the less possibility of structural damage with the new upgrading system.

Acknowledgements

The authors greatly appreciate the financial supports from the National Key Research and Development Program of China (Grant No. 2016YFC0701400), the National Natural Science Foundation of China (Grant Nos. 51525801, 51838004, 51708106), and the Natural Science Foundation of Jiangsu Province (Grant No. BK20170680).

Appendix A. Supplementary explanations for symbols used in the design procedure

Symbol	Explanation	Symbol	Explanation
A_b	Section areas of the brace	i^1_{b-r}	Line stiffness of the right beam on the first floor
A_c	Section areas of the column	i^1_c	Line stiffness of the calculated column on the first floor
A_{con}	Section areas of the concrete of the brace	K_{ce}	Lateral stiffness of the existing RCF column
A_e	Effective cross sectional areas of the anchor bolt	K_{cp}	Lateral stiffness of the outside precast column

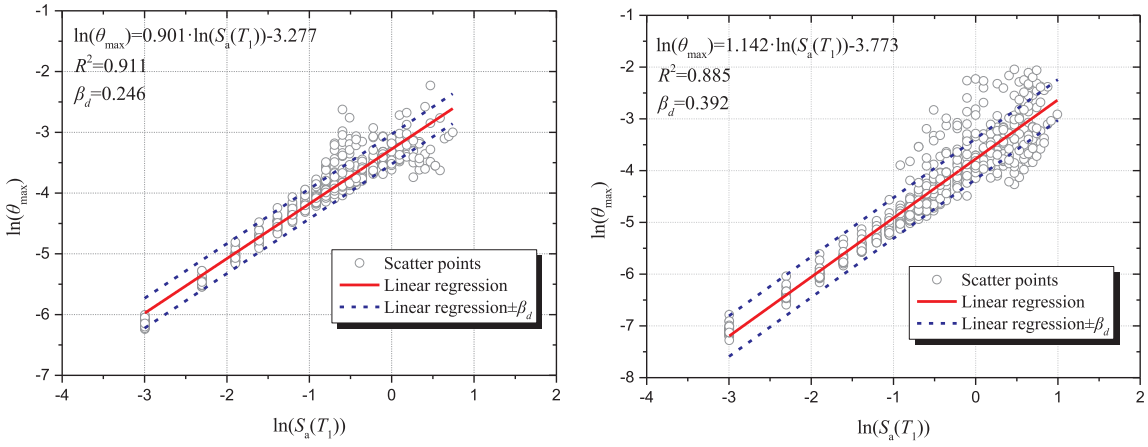

(a) EDP of θ_{max} before strengthening (b) EDP of θ_{max} after strengthening

Fig. 19. The linear regression of the log-transformed IM-EDP pairs.

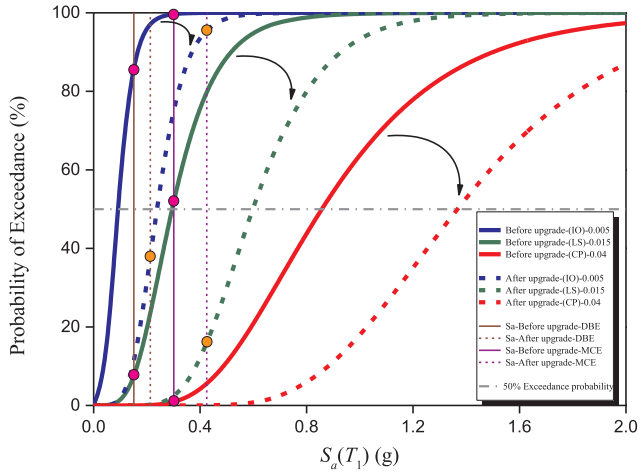

Fig. 20. Fragility curves before and after strengthening (EDP of θ_{max}).

Table 6
The intersections between the fragility curves and the corresponding target $S_a(T_1)$ under both the DBE and MCE.

Level	State	Period (s)	$S_a(T_1)$ (g)	Exceedance probability (%)		
				IO	LS	CP
DBE	Before	1.3459	0.151	85.6	7.7	0
	After	0.9186	0.213	37.9	0	0
MCE	Before	1.3459	0.301	99.6	52.1	0.97
	After	0.9186	0.425	95.4	15.9	0

E_b	Elastic modulus of the brace	K_{bt}	Lateral stiffness of the outside precast tensile brace
E_c	Elastic modulus of the column	K_{bc}	Lateral stiffness of the outside precast compressive brace
E_{con}	Elastic modulus of the concrete	K_b	Lateral stiffness of all the braces of the storey
F_{bcx}	Horizontal force of the compressive brace	$K_{initial}$	Initial lateral stiffness of the storey
F_{btx}	Horizontal force of the tensile brace	k_{bt}	Slope of the tensile point with the origin point
f_{con}	Compressive strength of the concrete	k_{bc}	Slope of the compressive point with the origin point
h	Storey height	L	Brace length
I_c	Moment of inertia of the column section in the earthquake direction	$Nc^n_{i\_b}$	Compressive capacity of the ith brace on the nth floor
$\bar{i}$	Line stiffness ratio between the beam and column	$Nt^n_{i\_b}$	Tensile capacity of the ith brace on the nth floor
i^n_{b-l}	Line stiffness of the left beam on the nth floor	n_f	Number of force friction surfaces
i^{n-1}_{b-l}	Line stiffness of the left beam on the $(n-1)$th floor	T_p	Pre-tension force of the high-strength friction bolt
i^n_{b-r}	Line stiffness of the right beam on the nth floor	μ	Anti-slip coefficient of the friction surface
i^{n-1}_{b-r}	Line stiffness of the right beam on the $(n-1)$th floor	θ	Angle between the brace and beam
i^n_c	Line stiffness of the calculated column on the nth floor	ψ_s	Seismic reduction coefficient of shear capacity of anchor bolts
i^1_{b-l}	Line stiffness of the left beam on the first floor		

References

[1] Qian K, Li B. Performance of three-dimensional reinforced concrete beam-column substructures under loss of a corner column scenario. J Struct Eng 2012;139(4):584–94.
[2] Qian K, Li B. Dynamic performance of rc beam-column substructures under the scenario of the loss of a corner column–experimental results. Eng Struct 2012;42:154–67.
[3] Feng D-C, Wu G, Lu Y. Numerical investigation on the progressive collapse behavior of precast reinforced concrete frame subassemblages. J Performance Construct Facilities 2018;32(3):04018027.
[4] Zhao X-L, Zhang L. State-of-the-art review on frp strengthened steel structures. Eng Struct 2007;29(8):1808–23.
[5] Pimanmas A, Chaimahawan P. Shear strength of beam–column joint with enlarged joint area. Eng Struct 2010;32(9):2529–45.
[6] Barnes R, Baglin P, Mays G, Subedi N. External steel plate systems for the shear strengthening of reinforced concrete beams. Eng Struct 2001;23(9):1162–76.
[7] Escórcio P, França PM. Experimental study of a rehabilitation solution that uses gfrp bars to replace the steel bars of reinforced concrete beams. Eng Struct 2016;128:166–83.
[8] Beigi HA, Sullivan TJ, Christopoulos C, Calvi GM. Factors influencing the repair costs of soft-story rc frame buildings and implications for their seismic retrofit. Eng Struct 2015;101:233–45.
[9] Mashhadiali N, Kheyroddin A. Seismic performance of concentrically braced frame with hexagonal pattern of braces to mitigate soft story behavior. Eng Struct 2018;175:27–40.
[10] Kake S, Kuramoto H, Castro JJ, Kagara M, Hiwatashi T, Abe T, et al. Shear transferring mechanisms of existing rc beams with an outside attached shear strengthening method (in japanese). J Struct Construct Eng 2014;79(695):113–20.
[11] Yamasaki K, Inai E, Akita T, Katagiri T, Osaki J, Kawamoto T, et al. Study on the seismic retrofitting method of existing reinforced concrete buildings by external frames(part.7)influence of the casting joints in the +-shaped beam-column joints of the external frame (in japanese). In: Proceedings of annual research meeting Chugoku Chapter, Architectural Institute of Japan (AIJ), vol. 39; 2016. p. 169–72. <https://ci.nii.ac.jp/naid/110010034258/en/>.
[12] Nakano T, Inai E, Akita T, Ozaki J, Komoto T, Kakihara T, et al. Study on the seismic retrofitting method of existing reinforced concrete building by external frames(part 11)lateral loading test of an external frame specimen. In: Proceedings of annual research meeting Chugoku Chapter, Architectural Institute of Japan (AIJ), vol. 39; 2016. p. 181–4. <https://ci.nii.ac.jp/naid/110010036176/en/>.
[13] Harayama K, Kawamoto T, Inai E, Matsukane Y. An experimental study of a seismic retrofitting method with framed steel brace systems partially and concentrically jointed with anchors. Proceedings of the 15th world conference on earthquake engineering. Tokyo, Japan: International Association for Earthquake Engineering; 2012.
[14] Terao Y, Kuroki M, Kikuchi K, Shimotsu K. Experimental study on bond behavior of main bars in r/c column with emergency retrofit by external prestressed pc rods: Part 6. Discussions on effect of rib pattern (in japanese), Kyushu chapter of architectural research meeting. Architect Inst Jpn (AIJ) 2016;55:505–8. <https://ci.nii.ac.jp/naid/110010026867/en/>.
[15] Tasai A, Nagayama K, Katsumata H, Sano T, Seki M. Strength of joint in seismic retrofit using outer-frame for existing rc buildings. Proceedings of the 13th world conference on earthquake engineering. Vancouver, Canada: International Association for Earthquake Engineering; 2004.
[16] Black CJ, Makris N, Aiken ID. Component testing, seismic evaluation and characterization of buckling-restrained braces. J Struct Eng 2004;130(6):880–94.
[17] Fahnestock LA, Ricles JM, Sause R. Experimental evaluation of a large-scale buckling-restrained braced frame. J Struct Eng 2007;133(9):1205–14.
[18] Jones AS. Low cost, light-weight buckling restrained braces for low rise buildings [Ph.D. thesis]. University of Auckland; 2011.
[19] Enomoto M, Kamiya T, Taguchi T, Haginoya M. Buildings research on new outside strengthening method contained steel plate concrete member: (part 21) experimental study of two-stories one-bay frame reinforced by steel tube brace (in japanese), Summaries of technical papers of annual meeting. Architect Inst Jpn (AIJ) 2011;2011:357–8<https://ci.nii.ac.jp/naid/110009519962/en/>.
[20] Priestley MN. Overview of presss research program. PCI J 1991;36(4):50–7.
[21] Kurama YC, Sritharan S, Fleischman RB, Restrepo JI, Henry RS, Cleland NM, et al. Seismic-resistant precast concrete structures: state of the art. J Struct Eng 2018;144(4):03118001.
[22] McKenna F, Fenves GL, Scott MH, et al. Open system for earthquake engineering simulation. Berkeley, CA: University of California; 2000.
[23] Mazzoni S, McKenna F, Scott MH, Fenves GL, et al. Opensees command language manual. Berkeley, CA: Pacific Earthquake Engineering Research (PEER) Center; 2007.
[24] Feng D-C, Ren X-D. Enriched force-based frame element with evolutionary plastic hinge. J Struct Eng 2017;143(10):06017005.
[25] Feng D-C, Ren X-D, Li J. Softened damage-plasticity model for analysis of cracked reinforced concrete structures. J Struct Eng 2018;144(6):04018044.
[26] Scott BD, Park R, Priestley M. Stress-strain behavior of concrete confined by overlapping hoops at low and high strain rates. J Proc 1982;79(1):13–27.
[27] Feng D-C, Li J. Stochastic nonlinear behavior of reinforced concrete frames. II: numerical simulation. J Struct Eng 2015;142(3):04015163.
[28] Feng D-C, Wu G, Lu Y. Finite element modelling approach for precast reinforced concrete beam-to-column connections under cyclic loading. Eng Struct 2018;174:49–66.
[29] Altoontash A. Simulation and damage models for performance assessment of reinforced concrete beam-column joints [Ph.D. thesis]. Palo Alto, California: Stanford University; 2004.
[30] Vecchio FJ, Collins MP. The modified compression-field theory for reinforced concrete elements subjected to shear. ACI J 1986;83(2):219–31.
[31] Bentz EC. Sectional analysis of reinforced concrete members [Ph.D. thesis]. Canada: University of Toronto; 2000.
[32] Feng D-C, Ren X, Li J. Implicit gradient delocalization method for force-based frame element. J Struct Eng 2015;142(2):04015122.
[33] Xu J, Feng D-C. Seismic response analysis of nonlinear structures with uncertain parameters under stochastic ground motions. Soil Dyn Earthquake Eng 2018;111:149–59.
[34] Feng D-C, Kolay C, Ricles JM, Li J. Collapse simulation of reinforced concrete frame structures. Struct Des Tall Special Build 2016;25(12):578–601.
[35] Zu X-J. Research on the seismic performance of existing concrete structures reinforced with externally attached precast beams and columns (in chinese) [Master's thesis]. Nanjing, China: Southeast university; 2016.
[36] Feng D-C, Xie S-C, Deng W-N, Ding Z-D. Probabilistic failure analysis of reinforced concrete beam-column sub-assemblage under column removal scenario. Eng Fail Anal 2019;100:381–92.
[37] Feng D-C, Wang Z, Wu G. Progressive collapse performance analysis of precast reinforced concrete structures. Struct Des Tall Special Build 2019;28(5):e1588https://doi.org/10.1002/tal.1588.
[38] FEMA (Federal Emergency Management Agency). Commentary for the seismic rehabilitation of buildings (FEMA-356), Washington, DC.; 2000.
[39] MHURD-PRC (Ministry of Housing and Urban-Rural Development of the People's Republic of China). Code for seismic design of buildings (GB50011), Beijing (in Chinese); 2010.
[40] MHURD-PRC (Ministry of Housing and Urban-Rural Development of the People's Republic of China). Technical Specification for Concrete Structures of Tall Building (JGJ3), Beijing (in Chinese); 2010.
[41] ICC (International Code Council). International building code (IBC), Country Club Hills, IL; 2006.
[42] ASCE (American Society of Civil Engineering). Minimum Design Loads for Buildings and Other Structures (ASCE/SEI 7-10), Reston, VA; 2010.
[43] MHURD-PRC (Ministry of Housing and Urban-Rural Development of the People's Republic of China). Code for design of steel structures (GB50017), Beijing (in Chinese); 2003.
[44] MHURD-PRC (Ministry of Housing and Urban-Rural Development of the People's Republic of China). Code for design of concrete structures (GB50010), Beijing (in Chinese); 2010.
[45] MHURD-PRC (Ministry of Housing and Urban-Rural Development of the People's Republic of China). Code for design of strengthening concrete structure (GB50367), Beijing (in Chinese); 2013.
[46] ATC of FEMA (Applied Technology Council of Federal Emergency Management Agency). Quantification of seismic performance factors (FEMA P-695), Washington, DC; 2009.
[47] Vamvatsikos D, Cornell CA. Incremental dynamic analysis. Earthquake Eng Struct Dyn 2002;31(3):491–514.
[48] Celik OC, Ellingwood BR. Seismic fragilities for non-ductile reinforced concrete frames–role of aleatoric and epistemic uncertainties. Struct Saf 2010;32(1):1–12.
[49] Jeon J, DesRoches R, Brilakis I, Lowes L. Modeling and fragility analysis of non-ductile reinforced concrete buildings in low-to-moderate seismic zones. Structures congress 2012. 2012. p. 2199–210.